

# CRYPTFLOW: Secure TensorFlow Inference

Nishant Kumar, Mayank Rathee, Nishanth Chandran, Divya Gupta, Aseem Rastogi and Rahul Sharma

Microsoft Research India

Email: {t-niskum, t-may, nichandr, Divya.Gupta, aseemr, rahsha}@microsoft.com

**Abstract**—We present CRYPTFLOW, a first of its kind system that converts TensorFlow inference code into Secure Multi-party Computation (MPC) protocols at the push of a button. To do this, we build three components. Our first component, *Athos*, is an end-to-end compiler from TensorFlow to a variety of semi-honest MPC protocols. The second component, *Porthos*, is an improved semi-honest 3-party protocol that provides significant speedups for TensorFlow like applications. Finally, to provide malicious secure MPC protocols, our third component, *Aramis*, is a novel technique that uses hardware with integrity guarantees to convert any semi-honest MPC protocol into an MPC protocol that provides malicious security. The security of the protocols output by *Aramis* relies on hardware for integrity and MPC for confidentiality. Moreover, our system, through the use of a new float-to-fixed compiler, matches the inference accuracy over the plaintext floating-point counterparts of these networks.

We experimentally demonstrate the power of our system by showing the secure inference of real-world neural networks such as RESNET50, DENSENET121, and SQUEEZENET over the ImageNet dataset with running times of about 30 seconds for semi-honest security and under two minutes for malicious security. Prior work in the area of secure inference (SecureML, MiniONN, HyCC, ABY<sup>3</sup>, CHET, EzPC, Gazelle, and SecureNN) has been limited to semi-honest security of toy networks with 3–4 layers over tiny datasets such as MNIST or CIFAR which have 10 classes. In contrast, our largest network has 200 layers, 65 million parameters and over 1000 ImageNet classes. Even on MNIST/CIFAR, CRYPTFLOW outperforms prior work.

## I. INTRODUCTION

Secure multiparty computation (or MPC) allows a set of mutually distrusting parties to compute a publicly known function on their secret inputs without revealing their inputs to each other. This is done through execution of a cryptographic protocol which guarantees that the protocol participants learn only the function output on their secret inputs and nothing else. MPC has made rapid strides - from being a theoretical concept three decades ago [62], [26], to now being on the threshold of having real world impact. One of the most compelling use cases for MPC is that of machine learning (ML) - e.g. being able to execute inference over ML algorithms securely when the model and the query are required to be hidden from the participants in the protocol. There has been a flurry of recent works aimed at running inference securely with MPC such as SecureML [45], MinioNN [42], HyCC [15], ABY<sup>3</sup> [44], CHET [20], EzPC [17], SecureNN [61], Gazelle [38], and so on. Unfortunately, these techniques are not easy-to-use by ML developers and have only been demonstrated on toy deep neural networks (DNNs) on tiny datasets such as MNIST or

CIFAR10. However, in order for MPC to be truly ubiquitous for secure inference tasks, it must be both effortless to use and capable of handling large ImageNet [23] scale DNNs.

In this work, we present CRYPTFLOW, a first of its kind system, that converts TensorFlow [3] inference code into secure computation protocols at the push of a button. By converting code in TensorFlow, a ubiquitous ML framework that is used in production by various technology companies, to secure computation protocols, we significantly lower the entry barrier for ML practitioners and programmers to use cryptographic MPC protocols in real world applications. We make the following four contributions:

- First, we provide a compiler, called *Athos*, from TensorFlow to a variety of secure computation protocols (both 2 and 3 party). In the absence of *Athos*, all prior works require *manually* re-implementing ML models in an MPC friendly low-level language/library, and hence, their evaluations have been limited to toy benchmarks where this task is feasible.
- Second, we provide a semi-honest secure 3-party computation protocol, *Porthos*, that outperforms all prior protocols for secure inference and enables us to execute, for the first time, the inference of ImageNet scale networks, that too in *about 30 seconds*.
- Third, assuming a minimally secure hardware which guarantees the integrity of computations, we show a novel technique, *Aramis*, that compiles any semi-honest secure MPC protocol to a malicious secure MPC protocol. *Aramis* only requires these integrity checks and no confidentiality guarantees for data residing within the hardware. The overhead of malicious security of *Aramis* based protocols is much lower compared to prior approaches, which enables the first implementations of DNN inference secure against malicious adversaries. Prior MPC protocols are either much slower than *Aramis* or fail to provide security against malicious adversaries.
- Fourth, we demonstrate the ease-of-use, efficiency and scalability of CRYPTFLOW by evaluating on
  - (a) RESNET50 [30], which won the ImageNet Large Scale Visual Recognition Challenge in 2015 [23];
  - (b) DENSENET121 [33], a convolutional neural network that won the best paper at CVPR 2017; and
  - (c) SQUEEZENET [35] with Fire modules.
 All these networks have heavily influenced the ML community with thousands of citations each. To demonstrate

that CRYPTFLOW is immediately useful in healthcare, we also evaluate CRYPTFLOW on DNNs used for prediction of lung diseases and diabetic retinopathy.

Our toolchain and all of our benchmarks are publicly available<sup>1</sup>. We now describe our results in more detail.

### A. Results

CRYPTFLOW outperforms prior work on ease-of-use, scalability, and efficiency. It automatically compiles TensorFlow code to MPC protocols with *no loss in classification accuracy*. This makes CRYPTFLOW the first secure inference system to produce a Top 1 accuracy of 76.45% and Top 5 accuracy of 93.23% for predictions running securely on the ImageNet dataset. Furthermore, in the 3-party setting, this can be done in about 30 seconds with semi-honest security and about 2 minutes with malicious security. Prior work in the area of secure inference ([45], [42], [15], [44], [20], [17], [38], [61]) has been limited to toy networks with 3–4 layers over tiny datasets such as MNIST or CIFAR which have 10 classes. Moreover, these implementations are limited to security against weaker semi-honest adversaries, that are assumed not to modify the code of the MPC protocol. In contrast, our largest network has 200 layers, 65 million parameters, over 1000 classes, and the user can choose between semi-honest and malicious security – the latter also protects against adversaries who can modify the code of the MPC protocol arbitrarily. Even on MNIST/CIFAR, CRYPTFLOW has lower communication complexity and is more efficient than prior and concurrent works [61], [44], [10]. Furthermore, CRYPTFLOW is the first system to implement<sup>2</sup> malicious security for secure DNN inference. We show that the overhead of Aramis over semi-honest protocols is small and varies between 25% and 3X depending on the size of the computation. Moreover, by very conservative estimates, Aramis based secure DNN inference is faster than state-of-the-art malicious secure MPC protocols [39] by at least an order of magnitude. Hence, on inference tasks, prior MPC protocols are either much slower than Aramis or fail to provide security against malicious adversaries. A summary of all our evaluation can be found in Section I-C.

### B. Components of CRYPTFLOW

We describe the three components of CRYPTFLOW next.

**Athos (Section III).** Athos is a compiler that compiles TensorFlow inference code to secure computation protocols. There are several challenges in doing so. First, for performance reasons all efficient secure computation protocols perform computation over fixed-point arithmetic – i.e., arithmetic over integers or arithmetic with fixed precision. This is in contrast to TensorFlow where computations are over floating-point values. Athos automatically converts TensorFlow code over floating-point values into code that computes the same function over fixed-point values. This compilation is done while matching the inference accuracy of floating-point code.

All prior works ([45], [42], [38], [44], [61]) in the area of running ML securely have performed this task by hand with great losses in accuracy. For example, it is trivial [2] to obtain a floating-point DNN with over 99% accuracy on classifying handwritten digits as 0, 1, . . . , 9. However, SecureML [45] works with a hand constructed fixed-point DNN which has only 94% accuracy to classify digits as 0 or 1. Although these fixed-point conversions are feasible to do manually for one or two toy benchmarks, this task quickly becomes intractable for large benchmarks and needs to be repeated for every new benchmark. Athos works by “sweeping through” various precision levels to estimate the best precision. The output of Athos is a sequence of function calls where each function can be implemented by an appropriate secure computation protocol, e.g., ABY [22] in the case of 2-party computation, Porthos for semi-honest secure 3-party computation and Aramis for malicious secure 3-party computation. This design of Athos addresses the challenge of modularity and makes it easy to incorporate new MPC protocols (Section III-C) and compiler optimizations (Section III-D).

**Porthos (Section IV).** Porthos is an improved semi-honest 3-party secure computation protocol (tolerating one corruption) that builds upon SecureNN [61]. Porthos makes two crucial modifications to SecureNN. First, SecureNN reduces convolutions to matrix multiplications and invokes the Beaver triples [11] based matrix multiplication protocol. When performing a convolution with filter size  $f \times f$  on a matrix of size  $m \times m$ , the communication is roughly  $2q^2f^2 + 2f^2 + q^2$  elements in the ring  $\mathbb{Z}_{2^{64}}$ , where  $q = m - f + 1$ . Porthos computes these Beaver triples by appropriately reshaping  $m \times m$  and  $f \times f$  matrices. This reduces the communication to roughly  $2m^2 + 2f^2 + q^2$  ring elements. Typically the filter size,  $f$ , is between 1 and 11 and the communication of Porthos can be up to two orders of magnitudes lower than SecureNN. Additionally, in SecureNN, the protocols for non-linear layers (such as Rectified Linear Units (ReLU) and MaxPool) require the third party to send secret shares to the first two parties. In Porthos, we cut this communication to half by eliminating the communication of one of these shares. This reduces the communication in the overall ReLU and MaxPool protocols by 25%. Thus, by reducing the communication in both linear convolution layers and non-linear layers, the communication in Porthos is several GBs lower than SecureNN (Table IX).

**Aramis (Section V).** Semi-honest secure MPC protocols assume that the protocol participants follow the protocol specification honestly and compute every message of the protocol correctly with respect to their input and the protocol history. On the other hand, maliciously secure MPC protocols make no such assumptions on the adversary and are guaranteed to be secure even when protocol participants deviate arbitrarily from the protocol. Obtaining maliciously secure MPC protocols through cryptography can often be challenging and expensive – typically some sort of “proof of honest computation” must be provided by the parties for every step of the protocol. We show a novel technique that uses hardware with integrity protection and compiles MPC protocols secure against semi-honest adversaries into MPC protocols that are secure against malicious adversaries. Our system, Aramis, only assumes a hardware with a) the integrity guarantee that once the code is attested, it cannot

<sup>1</sup><https://github.com/mpc-msri/EzPC>

<sup>2</sup>ABY<sup>3</sup> [44] provided a theoretical protocol to convert their semi-honest protocol into a malicious secure protocol on much smaller benchmarks than CRYPTFLOW, but did not provide an implementation or experimental validation.

be modified; and b) the ability to securely sign messages (without the host machine or party running the hardware being able to forge signatures). We formalize this secure hardware as an ideal functionality and show how it can be realized with Intel’s Software Guard Extensions (Intel SGX) [37]. This trust assumption on the secure hardware is significantly weaker than prior works on secure computation based on SGX [56], [52], [29], [9], [18] which assume that SGX completely hides all secrets from the host and even if data is decrypted and computed upon inside SGX, it cannot be viewed by the host. In contrast, in our adversarial model, the host can see all the data inside the hardware. Since we rely on semi-honest MPC for confidentiality, unlike prior works that use SGX, Aramis is naturally resistant to all side-channel attacks. To demonstrate the generality of Aramis, we compile both the semi-honest GMW (2 party protocol) [26] and Porthos (3 party protocol) to obtain malicious versions of these protocols. Porthos compiled with Aramis gives the first experimentally vetted maliciously secure protocol for neural network inference. Running interactive MPC protocols that perform memory intensive inference tasks in SGX with low overhead requires us to address various challenges that are discussed in Section V-D.

### C. Summary of empirical results

We list the claims empirically validated by this work:

- CRYPTFLOW is the first work to automatically run MPC protocols for ImageNet scale DNNs (Table IV) and realistic DNNs used in healthcare (Section VI-F). CRYPTFLOW compiles TensorFlow code to MPC protocols whose runtime and communication scale linearly with the depth of DNNs (Figure 10).
- MPC protocols for fixed-point are much more efficient than their floating-point counterparts (Table I). Therefore, CRYPTFLOW uses fixed-point arithmetic. Athos-generated fixed-point code matches classification accuracy of floating-point code (Table VII).
- The 2-party computation (2PC) protocols (ABY, CHET, MiniONN, EzPC, Gazelle) are much slower than the 3-party computation (3PC) protocols (Table VIII and Table VI). Thus, in CRYPTFLOW we focus on running the large benchmarks with Porthos, a 3PC protocol. Porthos has lower runtime and communication than prior 3PC works on secure inference (SecureNN [61] and ABY<sup>3</sup> [44]) (Table IX and Table V).
- Aramis is a general technique that can be used to port MPC protocols like GMW to SGX with minimal overhead (Table X). Aramis-based protocols for inference secure against malicious adversaries have about 3X overhead over the corresponding semi-honest secure protocols (Table IV). For inference tasks, Aramis is much more efficient than pure crypto-based approaches to malicious security (Section VI-E1).

### D. Organization of the paper

We provide an end-to-end walkthrough of our system to illustrate the overall toolchain in Section II. In Section III, we describe Athos, our float-to-fixed conversion method. Section

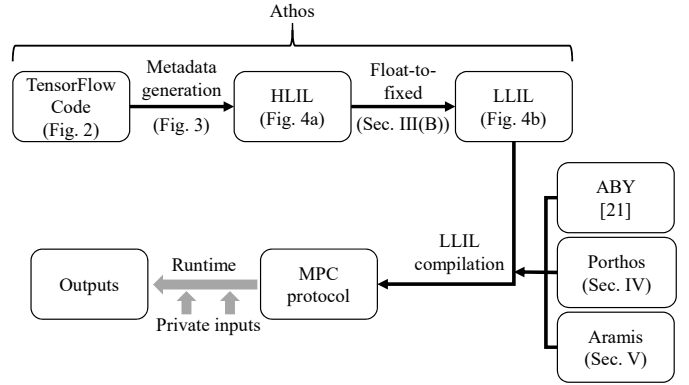


Fig. 1: CRYPTFLOW: End-to-end toolchain

IV describes our improved 3-party semi-honest secure protocol for neural networks. We describe Aramis that compiles any semi-honest secure protocol into a malicious secure protocol, in Section V. We present all our experimental results in Section VI, related works in Section VII and conclude in Section VIII.

## II. MOTIVATING EXAMPLE

In this section, we describe the end-to-end working of CRYPTFLOW through an example of logistic regression. The high level toolchain is shown in Figure 1. We describe, at a very high level, how code compilation happens from TensorFlow to secure computation protocols.

The CRYPTFLOW toolchain takes as input code written in vanilla TensorFlow. For example, consider the code snippet for logistic regression over MNIST dataset in TensorFlow as shown in Figure 2. Our compiler compiles this code to MPC protocols using the following sequence of steps. It first generates the TensorFlow graph dump (as shown in Figure 3a) as well as metadata to help compute the dimensions of all the tensors (Figure 3b). III-A provides more details on the frontend. Once this is done, the TensorFlow graph dump is compiled into a high-level intermediate language HLIL. The code snippet for logistic regression in HLIL is shown in Figure 4a. Next, Athos’ float-to-fixed converter translates the floating-point HLIL code to fixed-point code in a low-level intermediate language LLIL. This step requires Athos to compute the right precision to be used for maximum accuracy (Section III-B). Figure 4b shows the LLIL code snippet for logistic regression. The function calls in this sequence can be implemented with a variety of secure computation backends - e.g. ABY [22] for the case of 2-party secure computation, Porthos for the case of semi-honest 3-party secure computation (Section IV) and Aramis (Section V) for the malicious secure variant. Different backends provide different security guarantees and hence vary in their performance. For this example, the three backends take 414ms, 6.5ms, and 10.2ms respectively.

## III. ATHOS

Athos compiles ML inference code written in TensorFlow to MPC protocols. It has the following main components:

- *Frontend.* Athos frontend compiles TensorFlow code to a high-level intermediate language (HLIL). HLIL sup-

```
# x is an MNIST image of shape (1, 784).
# W and b are the model parameters.

print(tf.argmax(tf.matmul(x, W) + b, 1))
```

Fig. 2: Logistic Regression: TensorFlow snippet

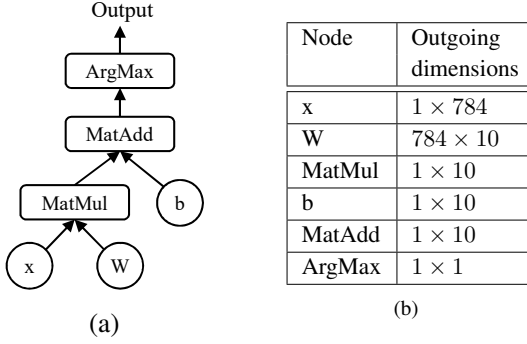


Fig. 3: Logistic Regression: (a) TensorFlow graph definition (b) Metadata consisting of graph nodes and their outgoing dimensions

ports floating-point tensors and sequence of function calls (corresponding to the TensorFlow nodes) that manipulate tensors. The main challenge in the frontend is to reconcile dynamic typing in TensorFlow to static typing in HLIL. TensorFlow code, written in Python, does not have tensor dimensions, whereas our HLIL has explicit tensor dimensions as it enables the compiler to perform optimizations.

- *Float-to-fixed converter.* While ML models use floating-point arithmetic, MPC protocols operate on fixed-point arithmetic. Rather than requiring the programmers to manually convert (or re-train) their models to integers, Athos performs the conversion automatically, without compromising on the inference accuracy.
- *Modular LLIL.* Athos compiles floating-point HLIL code to fixed-point code in a low-level intermediate language (LLIL). LLIL is a C-like imperative language that supports integer tensors, loops, conditionals, and functions. LLIL also makes it easier for different cryptographic backends to be plugged into Athos. It precisely specifies the interface that it requires the cryptographic protocols to

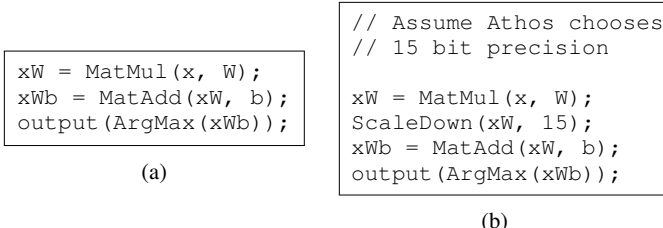


Fig. 4: Logistic Regression in (a) floating-point: HLIL syntax (b) fixed-point: LLIL syntax

implement, while providing a library for other operations. The LLIL is compiled down to the MPC protocol code.

- *Optimizations.* Athos implements MPC specific optimizations as well as several standard dataflow analyses and compiler optimizations. The design of HLIL and LLIL, and the choice of them being statically typed, is partly motivated by the requirements of these analyses.

Below we explain each of these components in detail.

#### A. Frontend and HLIL

Athos frontend compiles the input TensorFlow models to HLIL (described next) with explicit tensor dimensions. To obtain these dimensions, the frontend first runs TensorFlow code on one dummy input and generates TensorFlow metadata that has all the required information. The metadata is then translated to HLIL.

We discuss some details of the frontend. A plain dump of the TensorFlow metadata contains some nodes that are semantically irrelevant for actual inference, e.g. `identity`, `assign`, etc. To avoid representing these nodes in HLIL, we first prune the TensorFlow graph to remove such nodes, specifically we use the TensorFlow graph transform tool [1] for this purpose. Next, we carefully review each of the remaining (tens of) TensorFlow nodes and desugar them to HLIL, while keeping the number of functions in HLIL as small as possible. TensorFlow also supports “broadcasting” [58] that allows operations on tensors of incompatible dimensions and sizes. For example, due to broadcasting, addition of a four dimensional tensor with a one dimensional tensor is a valid operation. Athos frontend passes the broadcasting information to HLIL, which then accounts for it by compiling it to the appropriate LLIL library function call.

Constant	$n ::= 0 \mid 1 \mid 2 \mid \dots$
Float constant	$r ::= n.n$
Type	$\hat{r} ::= \text{float} \mid \text{int} \mid \hat{r}[n]$
Matrix	$\hat{M} ::= \bar{r} \mid \hat{M}$
Expression	$\hat{e} ::= n \mid x \mid \hat{M} \mid \hat{e}_1 \oplus \hat{e}_2 \mid x[\hat{e}]$
Program	$\hat{p} ::= \text{void main}() \{ \bar{r} \bar{x} ; f(\hat{e}) \}$

Fig. 5: HLIL syntax

Figure 5 shows the HLIL (we use  $\bar{r}$  to denote sequences of floating-point constants, and similarly for other syntactic categories). It is a simple language of floating-point tensors ( $\hat{M}$ ), with dimensions ( $n$ ) and sizes as explicit type annotations ( $\hat{r}[n]$ ), and the `main` is a sequence of variable declarations and function calls.

We next discuss how Athos performs float-to-fixed conversion on HLIL programs.

#### B. Float-to-fixed

As observed earlier, most ML models are expressed using floating-point, while MPC protocols operate on integers. For large models, we cannot expect the programmers to manually translate or re-train floating-point ML models to integer code (the common approach in literature on secure inference of toy

models [45], [42], [38], [44], [61]). Furthermore, it is well-known that floating-point operations are much more inefficient than fixed-point when evaluated securely ([45], [44]) – we re-confirm this by performing two-party secure multiplication [21] using both fixed-point and floating-point arithmetic to showcase the difference. This is illustrated in Table I which shows the huge overheads associated with floating-point arithmetic. In future, if efficient protocols for floating-point become available then we can directly compile HLIL to them, but until then Athos automatically performs the translation.

The translation is parametrized by a scale parameter  $s$  that determines the precision. We discuss how this scale is set later in the section. Given a scale  $s$ , we define a map  $\rho_s : \mathbb{R} \rightarrow \mathbb{Z}_{2^b}$  that maps Reals to  $b$ -bit integers:  $\rho_s(r) = \lfloor r \cdot 2^s \rfloor$ . We abuse notation and also apply  $\rho_s$  to matrices  $M$  of Reals where the result is a point-wise application of  $\rho_s$  to each matrix element. In the output fixed-point code, every Real number  $r$  is represented by a  $b$ -bit integer. The Real representation of an integer  $n$  is given by  $\frac{n}{2^s}$ . The float-to-fixed conversion (for interesting cases) is described in the following algorithm (ScaleDown is described in Table II):

$$\begin{aligned}
F(n) &= n \\
F(r) &= \rho_s(r) \\
F(\hat{M}) &= \rho_s(\hat{M}) \\
F(\text{float } x) &= \text{int } x \\
F(\text{MatAdd}(A, B, C)) &= \text{MatAdd}(A, B, C) \\
F(\text{MatMul}(A, B, C)) &= \text{MatMul}(A, B, C); \\
&\quad \text{ScaleDown}(C, s)
\end{aligned}$$

As an example of the conversion process, consider the program  $M_1 * M_2$  that multiplies the row vector  $M_1 = [400.1, 200.1]$  with the column vector  $M_2 = [0.3, 0.1]^T$ . Then in infinite precision Real arithmetic the result of the computation  $400.1 * 0.3 + 200.1 * 0.1$  is 140.04. Floating-point arithmetic only has a 23-bit mantissa and computes the approximately correct result 140.040009. When using Athos, the computed result can be much more precise than the floating-point result. We use  $0.1f$  to denote the floating-point number closest to the Real number 0.1. Given  $s = 24$ ,  $F(M_1 * M_2)$  results into the following program over integers

$$(\rho_{24}(400.1f) * \rho_{24}(0.3f) + \rho_{24}(200.1f) * \rho_{24}(0.1f)) / 2^{24}$$

which results in the following computation with 64-bit integers

$$(6712564224 * 3357121024 + 5033165 * 1677721) / 2^{24}$$

The final result is 2349481329 that represents the real number  $\frac{2349481329}{2^{24}} = 140.040000021457672119140625$  which is a better approximation than the floating-point result.

Athos, assigns the same bit-width  $b$  and the same scale  $s$  to all network parameters. While we could use different  $b$  and  $s$ , our experimental results show that same values for all parameters works quite well in-practice. We keep the scale public for efficiency: division with  $2^s$  when  $s$  is secret is much more expensive than when  $s$  is public. Moreover, scaling down operations (division by  $2^s$ ) cause loss of precision, as they lose significant bits, and hence need to be minimized. Therefore, Athos scales down only once per matrix multiplication and does not scale down matrix additions.

# Sequential Multiplications	Fixed (ms)	Float (ms)	Overhead
1	2.57	72.35	28.11x
10	4.88	278.8	57.1x
100	21.65	2735	126.34x
1000	199.6	25281.42	126.6x

TABLE I: Floating-point vs Fixed-point multiplication.

While we use machine integer width (64) for  $b$ , finding a good value of  $s$  is difficult. We explain the various tradeoffs that govern the choice of  $s$  and then discuss our solution.

Suppose, in our example,  $s$  is set too low:  $s = 2$ . Then  $F([400.1f, 200.1f] * [0.3f, 0.1f])$  is

$$(1600 * 1 + 800 * 0) / 4$$

which represents the Real number  $400/4 = 100$ . This result is far from 140.04. Here, low scale values have lead to loss of significant bits. In particular, 0.1 has been rounded to zero causing an imprecise result. Ideally we want to set the scale to a large value so that the integers have many significant digits.

Next, suppose  $s$  is set to a very high value, e.g., 60. Then, the computation  $\rho_{60}(400.1f) * \rho_{60}(0.3f)$  overflows 64-bit integers and the result is garbage (multiplication of these two large positive numbers would become a negative number).

Thus, scale can neither be very low nor very high; we need to find a sweet spot. To determine an appropriate value of  $s$ , we sweep over all its possible values  $\{0, 1, \dots, b - 1\}$  and choose the value that leads to the best accuracy. For the example  $400.1f * 0.3f + 200.1f * 0.1f$ , the most accurate result is obtained at  $s = 24$ . In general, machine learning algorithms have a validation dataset which is used for hyperparameter tuning. We consider scale as a hyperparameter and select the scale that leads to a fixed-point classifier implementation which performs the best on the validation set. This scheme helps us select values of scales that result in minimal accuracy loss.

### C. Modular LLIL

Constant	$n ::= 0 \mid 1 \mid 2 \mid \dots$
Type	$\tau ::= \text{int} \mid \tau[n]$
Matrix	$M ::= \bar{n} \mid \bar{M}$
Expression	$e ::= n \mid x \mid M \mid e_1 \oplus e_2 \mid x[e]$
Statement	$s ::= \tau x \mid x = e \mid \text{for}(x = e_1; x < e_2; x++) \{s\}$ $\mid x[e_1] = e_2 \mid \text{if}(e, s_1, s_2) \{s_1; s_2\} \mid \text{return } e$ $\mid f(\bar{e}) \mid d(\bar{e})$
Global	$g ::= \text{extern } \tau d(\bar{\tau x}) \mid \tau f(\bar{\tau x}) \{s\}$
Program	$p ::= \bar{g}; \text{void main}() \{s\}$

Fig. 6: LLIL syntax

Athos compiles HLIL to LLIL, a crypto-aware, C-like intermediate language that has only integer-valued tensors. Figure 6 shows the syntax of LLIL.

This language is a subset of C and has sufficient expressiveness required to implement ML inference tasks. In particular it supports arrays, basic arithmetic, loops, branching, functions, and `extern` declarations. LLIL makes the Athos interface to the MPC cryptographic protocols explicit. We observe that the tensor operations in a typical TensorFlow code fall into

two categories: those that do not change the values but just copy the data around (e.g. `squeeze` to remove dimensions of size 1 from a tensor, `pad` to pad a tensor with various kinds of paddings, `transpose` to take the transpose of a tensor, and `concat` to concatenate two tensors into a single tensor), and those that compute new values. For functions that do not manipulate shares (denoted by  $f$ ), LLIL provides a library with their implementations that is automatically added as a prelude to LLIL programs. Changing the underlying crypto protocol does not require changes to these library functions and this library can be used by all crypto developers. These functions are implemented in LLIL and are compiled to C++ code.

Share-manipulating functions (`extern d`) are required to be implemented in the cryptographic backend. All a crypto developer needs to do is to implement these functions, and then she would be able to directly evaluate the protocols on ML models used in practice. We describe these functions with their signatures and intended semantics in Table II. Concretely, we provide three implementations of these functions: using the 2PC protocols of ABY [22], 3PC protocols of SecureNN [61], and Porthos (Section IV).

Finally, Athos compiles LLIL programs to C and links them with the cryptographic MPC protocol implementation.

#### D. Optimizations

Athos intermediate languages are designed to be amenable to static analysis. In particular, we have implemented several standard dataflow analyses and compiler optimizations [6]: reaching definitions, liveness analysis, and so on. These analyses help with optimizing memory utilization and we have observed savings reaching upto 80%. To demonstrate the ease of implementing analyses and optimizations, we provide an example each: (a) a peephole optimization ReLU MaxPool Switching on HLIL to improve efficiency of DNNs that use ReLU and MaxPool, and (b) an analysis Counting Scale Down operations on LLIL to determine the number of scale down operations done in order to prevent loss in accuracy (a similar analysis was done manually in [45], [61], [44]).

1) *ReLU MaxPool Switching*: The ReLU operation is one of the most time intensive task in secure inference of DNNs. For some DNNs, secure evaluation of ReLUs can consume upto 80% of the total protocol execution time. This is in contrast to evaluation in the clear where ReLUs consume only a fraction of the total time. Hence, it is plausible that ML developers can write TensorFlow code in a way that has no impact on cleartext evaluation but can severely degrade the performance of secure evaluation. One such idiom involves applying ReLU to a matrix followed by MaxPool. Notice that ReLU and MaxPool are commutative operators:  $\text{ReLU}(\text{MaxPool}(\cdot))$  is functionally equivalent to  $\text{MaxPool}(\text{ReLU}(\cdot))$ . Moreover, for cleartext performance, there is no discernible difference in the performance of these two alternatives. Hence, most TensorFlow developers have adopted the convention of  $\text{MaxPool}(\text{ReLU}(\cdot))$ .

For secure evaluation,  $\text{MaxPool}(\text{ReLU}(\cdot))$  can be much more inefficient than  $\text{ReLU}(\text{MaxPool}(\cdot))$  as this significantly reduces the number of ReLU operations that need to be performed in MPC. Hence, we have built an optimization pass on HLIL that replaces occurrences of  $\text{MaxPool}(a, b, \text{ReLU}(A))$ ;

with  $\text{ReLU}(\text{MaxPool}(a, b, A))$ . For example, if the input matrix  $A$  has dimensions  $112 \times 112 \times 64$  and we compute a MaxPool with  $2 \times 2$  windows. Then, the output matrix has dimensions  $56 \times 56 \times 64$ . Hence, the latter needs to compute only one fourth the number of ReLUs compared to the former. In this case, the optimized code is over  $3 \times$  better in communication and over  $2 \times$  faster in our experimental setup (Section VI).

2) *Counting Scale Down operations*: We describe an analysis to count the number of scale down operations in an LLIL code. The analysis uses an environment  $\rho$  that maps tensors to the number of elements they contain. This environment is populated using variable declarations in the code. The analysis makes a single pass over `main` and for each call `ScaleDown(A, s)` accumulates  $\rho(A)$  into a counter. The final value of the counter provides the number of scale down operations in the code.

Note that this analysis is easy to describe as the LLIL code contains dimensions of all the tensors explicitly. Hence, the compiler can statically populate  $\rho$ . This analysis is impossible to perform on the TensorFlow Python code as the sizes of tensors are unknown at compile time.

## IV. PORTHOS

We now describe Porthos, our improved secure 3PC protocol that provides semi-honest security against one corrupted party and privacy against one malicious corruption. The notion of privacy against malicious corruption (introduced by Araki *et al.* [8]) informally guarantees that privacy of inputs hold even against malicious party as long as none of the parties participating in the protocol learn the output of the computation (this is relevant for example, when computation is offloaded to servers). Porthos builds upon SecureNN [61] but makes crucial modifications to reduce communication. We first describe our protocols that reduce communication and summarize concrete improvements in Table III.

We reduce communication for both linear as well as non-linear layers of DNNs. Linear layers include fully connected layers as well as convolutional layers. We improve the communication for convolutional layers and our optimization gains get better with larger filter sizes. With regards to non-linear layers (ReLU and MaxPool), we modify how two of the protocols in SecureNN are used – ComputeMSB and ShareConvert. As we explain below, this directly translates to better communication for both ReLU and MaxPool computations. At a very high level, we trade communication with compute by modifying the way certain shares are generated in the protocol.

**Convolution.** In SecureNN, secure computation of convolutional layers is done by reducing them to a (larger) matrix multiplication. As an example, 2-dimensional convolution of a  $3 \times 3$  input matrix  $X$  (with single input channel and stride 1) with a filter  $Y$  of size  $2 \times 2$  reduces to a matrix multiplication as follows:

$$\text{Conv2d} \left( \begin{bmatrix} x_1 & x_2 & x_3 \\ x_4 & x_5 & x_6 \\ x_7 & x_8 & x_9 \end{bmatrix}, \begin{bmatrix} y_1 & y_2 \\ y_3 & y_4 \end{bmatrix} \right) = \begin{bmatrix} x_1 & x_2 & x_4 & x_5 \\ x_2 & x_3 & x_5 & x_6 \\ x_4 & x_5 & x_7 & x_8 \\ x_5 & x_6 & x_8 & x_9 \end{bmatrix} \times \begin{bmatrix} y_1 \\ y_2 \\ y_3 \\ y_4 \end{bmatrix}$$

MatMul(int[L][M] A, int[M][N] B, int[L][N] C)	Multiply two tensors $A$ and $B$ and store results in $C$
MatAdd(int[L][M] A, int[L][M] B, int[L][M] C)	Add two tensors $A$ and $B$ into $C$
Conv(int[H][W][CI] A, int[FW][CW][CO] F)	Convolve a tensor $A$ with filter $F$
Avg/Max Pool(a, b, int[H][W][C] A)	Apply a stencil that computes the average/max value in windows of size $a \times b$ of tensor $A$ .
ArgMax(int[M] A)	Compute the index with maximum value in $A$
FusedBatchNorm(int[K][L][M][N] A, int[N] B, int[N] C)	Returns $\forall k, l, m, n. B[n] \times A[k][l][m][n] + C[n]$
ReLU(int[M][N] A)	Returns $\forall i, j. \text{Max}(A[i][j], 0)$
ScaleDown(int[M][N] A, k)	Divide each entry of $A$ with $2^k$ .

TABLE II: Share manipulating functions. These have been simplified for exposition by suppressing parameters such as padding and strides. For comprehensive signatures, see [https://www.tensorflow.org/api\\_docs/python/tf/](https://www.tensorflow.org/api_docs/python/tf/).

In the above matrix multiplication, we call the left matrix (derived from  $X$ ) as the “reshaped input” (say,  $X'$ ) and the right matrix (derived from  $Y$ ) as the “reshaped filter” (say,  $Y'$ ). The matrix multiplication is computed securely using a matrix Beaver triple [11], [45] based protocol. Later, the output can be reshaped to get the output of convolution in correct shape. In this protocol, matrices being multiplied are masked by random matrices of same size and communicated and hence, the communication grows with the size of the matrices. We observe that this is quite wasteful for convolution because the reshaped input image (the first matrix in multiplication) has many duplicated entries (e.g.,  $x_2$  in row 1 and row 2) that get masked by independent random values. Let size of  $X$  be  $m \times m$  and size of  $Y$  be  $f \times f$ . Then, the size of  $X'$  is  $q^2 \times f^2$ , where  $q = m - f + 1$ . In Porthos, we optimize the size of matrix based Beaver triples for convolution by exploiting the structure of re-use of elements as the filter moves across the image. At a high level, we pick random matrix of size matching  $X$  for masking and communication only grows with size of  $X$  (i.e.,  $m^2$ ) instead of  $X'$  (i.e.,  $q^2 f^2$ ) in SecureNN.

Before, we describe our optimized protocol, we set up some notation. Let  $\langle x \rangle_0^t$  and  $\langle x \rangle_1^t$  denote the two shares of a 2-out-of-2 additive secret sharing of  $x$  over  $\mathbb{Z}_t$  – in more detail, pick  $r \xleftarrow{\$} \mathbb{Z}_t$ , set  $\langle x \rangle_0^t = r$  and  $\langle x \rangle_1^t = x - r \pmod t$ .  $\langle x \rangle^t$  denotes a sharing of  $x$  over  $\mathbb{Z}_t$ . Reconstruction of a value  $x$  from its shares  $x_0$  and  $x_1$  is simply  $x_0 + x_1$  over  $\mathbb{Z}_t$ . This generalizes to larger dimensions - e.g. for the  $m \times n$  matrix  $X$ ,  $\langle X \rangle_0^t$  and  $\langle X \rangle_1^t$  denote the matrices that are created by secret sharing the elements of  $X$  component-wise (other matrix notation such as  $\text{Reconst}^t(X_0, X_1)$  are similarly defined).

Let  $\text{Conv2d}_{m,f}$  denote a convolutional layer with input  $m \times m$ , 1 input channel, a filter of size  $f \times f$ , and 1 output channel. Our protocol for  $\text{Conv2d}_{m,f}$  is described in Algorithm 1, where  $L = 2^\ell$ ,  $\ell = 64$ . Algorithms  $\text{ReshapeInput}$ ,  $\text{ReshapeFilter}$  and  $\text{ReshapeOutput}$  are used to reshape input, filter and output as described above and are formally described in Appendix A. Parties  $P_0$  and  $P_1$  start with shares of input matrix  $X$  and filter  $Y$  over  $\mathbb{Z}_L$ . That is,  $P_j$  holds  $(\langle X \rangle_j^L, \langle Y \rangle_j^L)$  for  $j \in \{0, 1\}$ . In SecureNN,  $P_0$  first reshapes  $\langle X \rangle_0^L$  into  $\langle X' \rangle_0^L$  by running  $\text{ReshapeInput}$ . Then, it picks a random matrix  $\langle A' \rangle_0^L$  of same size as  $X'$  and sends  $\langle E' \rangle_0^L = \langle X' \rangle_0^L - \langle A' \rangle_0^L$  to  $P_1$  that requires communicating  $q^2 f^2$  elements. In Porthos, we optimize this as follows:  $P_0$  picks a random matrix  $\langle A \rangle_0^L$  of same size as  $X$  (Step 1) and sends  $\langle E \rangle_0^L = \langle X \rangle_0^L - \langle A \rangle_0^L$  to  $P_1$  (Step 4) that requires communicating  $m^2$  elements only. Later, parties can reshape  $E$  locally to get  $E'$ . We reduce the communication by  $P_1$  in a symmetric manner. Concretely, we reduce communication from  $(2q^2 f^2 + 2f^2 + q^2)\ell$  in SecureNN to  $(2m^2 + 2f^2 + q^2)\ell$ . This algorithm can be easily generalized

to the setting where there are  $i$  input filters,  $o$  output filters, and different stride and padding parameters.

---

**Algorithm 1:** 3PC protocol for  $\text{Conv2d}_{m,f}$

---

**Input:**  $P_0$  holds  $(\langle X \rangle_0^L, \langle Y \rangle_0^L)$  and  $P_1$  holds  $(\langle X \rangle_1^L, \langle Y \rangle_1^L)$ , where  $X \in \mathbb{Z}_L^{m \times m}$ ,  $Y \in \mathbb{Z}_L^{f \times f}$ .

**Output:**  $P_0$  gets  $\langle \text{Conv2d}_{m,f}(X, Y) \rangle_0^L$  and  $P_1$  gets  $\langle \text{Conv2d}_{m,f}(X, Y) \rangle_1^L$ .

**Common Randomness:**  $P_0$  &  $P_1$  hold shares of a zero matrix  $U$  of dimension  $q \times q$ ,  $q = m - f + 1$ .  $P_0$  &  $P_2$  hold a common PRF key  $k_0$ , and  $P_1$  &  $P_2$  hold a common PRF key  $k_1$ .

- 1)  $P_0$  &  $P_2$  use PRF key  $k_0$  to generate random matrices  $\langle A \rangle_0^L \in \mathbb{Z}_L^{m \times m}$ ,  $\langle B \rangle_0^L \in \mathbb{Z}_L^{f \times f}$  and  $\langle C \rangle_0^L \in \mathbb{Z}_L^{q \times q}$ .
- 2)  $P_1$  &  $P_2$  use PRF key  $k_1$  to generate random matrices  $\langle A \rangle_1^L \in \mathbb{Z}_L^{m \times m}$  and  $\langle B \rangle_1^L \in \mathbb{Z}_L^{f \times f}$ .
- 3)  $P_2$  computes  $A = \langle A \rangle_0^L + \langle A \rangle_1^L$  and  $B = \langle B \rangle_0^L + \langle B \rangle_1^L$ . Let  $A' = \text{ReshapeInput}(A)$  and  $B' = \text{ReshapeFilter}(B)$ .  $P_2$  computes  $\langle C' \rangle_1^L = A' \cdot B' - \langle C \rangle_0^L$  and sends it to  $P_1$ .
- 4) For  $j \in \{0, 1\}$ ,  $P_j$  computes  $\langle E \rangle_j^L = \langle X \rangle_j^L - \langle A \rangle_j^L$  and  $\langle F \rangle_j^L = \langle Y \rangle_j^L - \langle B \rangle_j^L$  and sends to  $P_{j+1}$ .
- 5)  $P_0$  &  $P_1$  reconstruct  $E$  and  $F$  using exchanged shares.
- 6) For  $j \in \{0, 1\}$ ,  $P_j$  computes  $\langle X' \rangle_j^L = \text{ReshapeInput}(\langle X \rangle_j^L)$ ,  $E' = \text{ReshapeInput}(E)$ ,  $\langle Y' \rangle_j^L = \text{ReshapeFilter}(\langle Y \rangle_j^L)$ ,  $F' = \text{ReshapeFilter}(F)$ .
- 7) For  $j \in \{0, 1\}$ ,  $P_j$  computes  $\langle Z' \rangle_j^L = -jE' \cdot F' + \langle X' \rangle_j^L \cdot F' + E' \cdot \langle Y' \rangle_j^L + \langle C \rangle_j^L + \langle U \rangle_j^L$ .
- 8) For  $j \in \{0, 1\}$ ,  $P_j$  outputs  $\langle Z \rangle_j^L = \text{ReshapeOutput}(\langle Z' \rangle_j^L)$ .

---

**Activation Functions.** In SecureNN protocols for computing activations such as ReLU and MaxPool start with parties  $P_0$  and  $P_1$  having shares of values over  $L = 2^{64}$ . For both of these, parties run a protocol called  $\text{ComputeMSB}$  to evaluate most significant bit (MSB) of secret values. This protocol require shares over  $L - 1$ . So parties run a protocol called  $\text{ShareConvert}$  to convert shares over  $L$  to shares over  $L - 1$ . Both protocols  $\text{ComputeMSB}$  and  $\text{ShareConvert}$  require  $P_2$  to send fresh shares of a value to  $P_0$  and  $P_1$ . In SecureNN, both of these shares were picked by  $P_2$  and explicitly communicated to  $P_0$  and  $P_1$ . As mentioned before, shares of a value  $x$  are  $r$  and  $x - r$ , where  $r$  is a appropriately picked uniformly random value. We observe that since one of the shares is truly random, it can be computed as the output of a shared PRF key between  $P_2$  and one of the parties, say  $P_0$ . This cuts the communication of this step to *half*. Moreover, since many activations are computed in parallel, we can carefully “load-balance” this optimization between  $P_0$  and  $P_1$  to reduce

Protocol	Communication (SecureNN)	Communication (Porthos)
Conv2d <sub>m,i,f,o</sub>	$(2q^2f^2i + 2f^2oi + q^2o)\ell$	$(2m^2i + 2f^2oi + q^2o)\ell$
ShareConvert	$4\ell \log p + 6\ell$	$3\ell \log p + 5\ell$
ComputeMSB	$4\ell \log p + 13\ell$	$3\ell \log p + 9\ell$
ReLU	$8\ell \log p + 24\ell$	$6\ell \log p + 19\ell$
MaxPool <sub>n</sub>	$(8\ell \log p + 29\ell)(n - 1)$	$(6\ell \log p + 24\ell)(n - 1)$

TABLE III: Communication complexity of protocols;  $q = m - f + 1$  and  $\log p = 8$ .

the communication to half on the critical path. We note that this optimization reduces the overall communication of ShareConvert, ComputeMSB, ReLU and MaxPool by 25%.

The revised table with comparison of overall communication complexity of all protocols with improvements over SecureNN are provided in Table III. Conv2d<sub>m,i,f,o</sub> denotes a convolutional layer with input  $m \times m$ ,  $i$  input channels, a filter of size  $f \times f$ , and  $o$  output channels. MaxPool<sub>n</sub> computes the maximum value out of a list of  $n$  elements.  $p$  denotes a prime value larger than 65 (set to 67 in SecureNN), with 8 bits being used to represent elements in  $\mathbb{Z}_p$  (hence  $\log p = 8$  in the table).

## V. ARAMIS

In this section, we describe Aramis, a general technique to convert any semi-honest secure MPC protocol into a secure MPC protocol tolerating malicious corruptions. The threshold of corrupted parties tolerated by the semi-honest protocol is retained in the malicious secure protocol by our technique. Aramis makes a very minimal trust assumption of *integrity* on hardware: the code and data residing in the hardware cannot be modified by the adversary. This implicitly requires the hardware to possess a trusted component that can produce signatures and this signature scheme cannot be forged by an adversary. We do not assume confidentiality, that is, the adversary can see all the code and user data that resides in the hardware belonging to the corrupted parties. This significantly weakens the trust assumption on hardware.

**Overview.** At a very high level, Aramis exploits the following (well-known) observation: in order for a semi-honest protocol to be made maliciously secure, one must ensure that all messages sent by every party  $P_i$  are computed honestly according to the specification of the semi-honest protocol consistent with  $P_i$ 's input and the transcript so far. The next observation we make is that if party  $P_i$  possesses hardware whose code can be attested by party  $P_j$  (and vice-versa), then  $P_j$  can obtain guarantees on the correctness of protocol messages sent by  $P_i$  as long as these messages are computed and signed by  $P_i$ 's hardware. Using these observations, we can convert a semi-honest secure protocol into one that is maliciously secure by having every protocol message of  $P_i$  be computed by the trusted hardware that  $P_i$  executes. We shall now describe our techniques in more detail. We first describe the ideal functionality that is assumed out of the hardware in Section V-A. We then describe our technique in Section V-B. Finally, we explain how Intel SGX can realize the ideal functionality in Section V-C and challenges in porting semi-honest MPC protocols to SGX in Section V-D.

### A. The attestation ideal functionality $\mathcal{F}_{\text{attest}}$

**Description.** We formally define the ideal functionality for attested executions in Figure 7. The functionality is parameter-

ized by a signing key pair  $(\text{vk}, \text{sk})$ . Let  $\text{Sign}_{\text{sk}}(m)$  denote the signing algorithm on message  $m$  and  $\text{Verify}_{\text{vk}}(m, \sigma)$  denote verification of signature  $\sigma$  on message  $m$ . At a high level, this functionality allows users to specify a function  $g$  to the ideal functionality once using the Commit command. The functionality returns a token  $\mathcal{T}_g$  generated as  $\text{Sign}_{\text{sk}}(H(g))$ , where  $H$  is a collision resistant hash function. Note that this token is publicly verifiable given  $g$  and  $\text{vk}$ . Let  $\text{state}_{\text{ctr}}$  be an internal state that the functionality maintains, indexed by  $\text{ctr}$  – this state can be maintained by signing it along with  $\text{ctr}$  and verifying the signature of the state on every input message. When the functionality  $\mathcal{F}_{\text{attest}}$  is initialized, the initial state  $\text{state}_0$  is empty (or,  $\epsilon$ ). Subsequent invocations of the functionality is done on input  $w_{\text{ctr}}$  using the Compute command. The function  $g$  is a deterministic mapping from  $(\text{ctr}, w_{\text{ctr}}, r_{\text{ctr}}, \text{state}_{\text{ctr}-1})$  to  $(y_{\text{ctr}}, \text{state}_{\text{ctr}})$ , where  $r_{\text{ctr}}$  is the required randomness. The functionality picks randomness  $r_{\text{ctr}}$ , evaluates  $g$  and provide a signature on the function output  $y_{\text{ctr}}$  using the signing key  $\text{sk}$ . Furthermore,  $(y_{\text{ctr}}, \text{state}_{\text{ctr}})$  is always given to party  $P$  such that  $\text{state}_{\text{ctr}}$  contains  $r_{\text{ctr}}$  in clear and this ensures that there is no information hidden from  $P$  and we only assume correct execution of  $g$ . That is, the ideal functionality can evaluate functions and provide signed outputs and these outputs could have anyway been computed by party  $P$  given knowledge of  $g, w_{\text{ctr}}, r_{\text{ctr}}, \text{ctr}, \text{state}_{\text{ctr}}$ , which are all known to  $P$ . Thereby, we only assume that the functionality will sign the output of  $g$  on the appropriate input and not hide any data from  $P$ . This significantly weakens what is assumed from the trusted hardware.

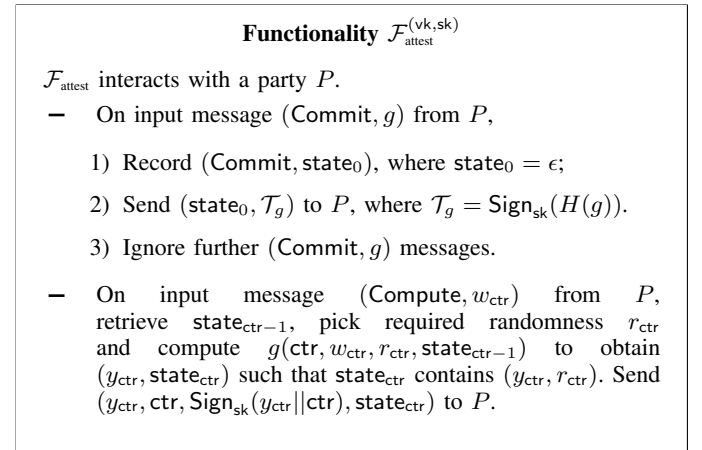


Fig. 7: The Authentication functionality  $\mathcal{F}_{\text{attest}}^{(\text{vk}, \text{sk})}$ .

### B. Semi-honest security to malicious security

Our technique takes any semi-honest secure MPC protocol and converts it into a malicious secure MPC protocol in the  $\mathcal{F}_{\text{attest}}^{(\text{vk}, \text{sk})}$ –hybrid model. The idea is to have messages sent by every party  $P_i$  to every other party  $P_j$  in the semi-honest protocol be computed by the corresponding  $\mathcal{F}_{\text{attest}}^{(\text{vk}_i, \text{sk}_i)}$  functionality interacting with  $P_i$ , where  $(\text{vk}_i, \text{sk}_i)$  are keys used by the functionality. These messages can be verified by functionality  $\mathcal{F}_{\text{attest}}^{(\text{vk}_j, \text{sk}_j)}$  interacting with  $P_j$ . We assume that every  $\mathcal{F}_{\text{attest}}^{(\text{vk}_j, \text{sk}_j)}$  knows the verification key  $\text{vk}_j$  used by functionalities of all other parties  $P_j$  in a reliable manner.

Later, we show how to achieve this through the use of remote attestation in the context of Intel SGX. We now set notation and describe the next message function of any semi-honest secure MPC protocol and how we modify it for our use.

**Next message function.** Let  $\pi(\cdot)$  be the next message function of any semi-honest secure MPC protocol.  $\pi(\cdot)$  takes the following values as input - two party ids  $i$  and  $j$ , input  $x_i$ , a round number  $\text{ctr}$ , randomness  $r_{i,j,\text{ctr}}$  and  $\text{Transcript}_i$ , which includes the transcript of all messages sent and received by the party  $P_i$  so far. Given these,  $\pi(\cdot)$  outputs  $y_{\text{ctr}}^{i,j}$ , which is the message that  $P_i$  must send to  $P_j$  in round  $\text{ctr}$  and also updates  $\text{Transcript}_i$  appropriately. Additionally,  $\pi(\cdot)$  takes message  $y_{\text{ctr}}^{j,i}$  sent by  $P_j$  to  $P_i$  at round  $\text{ctr}$  and update  $\text{Transcript}_i$  with this message. We now describe how to modify  $\pi(\cdot)$  to  $\pi^*(\cdot)$  to incorporate checks to detect malicious behaviour.

**Modified next message function.**  $\pi^*(\cdot)$ , is the modified function that builds upon  $\pi(\cdot)$  and we describe it for  $P_i$ .

- 1) For  $\text{ctr} = 1$ , Let  $x_i$  be the input of  $P_i$  in  $\pi(\cdot)$ . Then,  $(\text{ctr}, x_i)$  is stored as  $\text{state}_1$  (also called as  $\text{Transcript}_i^1$ ) and sent to  $P_i$ .
- 2) When  $\pi^*(\cdot)$  receives a message  $M = (y_{\text{ctr}}^{j,i}, \text{ctr}, \sigma)$  from party  $P_j$ , it runs  $\text{Verify}_{\text{vk}_j}((y_{\text{ctr}}^{j,i}, \text{ctr}), \sigma)$ . If verification succeeds, it appends  $M$  to  $\text{Transcript}_i$ . Else,  $P_i$  aborts.
- 3)  $\pi^*(\cdot)$  on input  $(\text{ctr}, \text{state}_{\text{ctr}-1}, j)$  computes the next message from  $P_i$  to  $P_j$  as follows: It checks that  $\text{state}_{\text{ctr}-1}$  contains a valid transcript of all messages computed so far. If it verifies, it picks randomness  $r_{i,j,\text{ctr}}$  and runs  $\pi(\text{ctr}, \text{state}_{\text{ctr}-1}, j, r_{i,j,\text{ctr}})$  to compute next message  $y_{\text{ctr}}^{i,j}$  and updated state  $\text{state}_{\text{ctr}}$  (containing  $r_{i,j,\text{ctr}}$ ). Else it outputs  $\perp$ . Note that  $\text{state}_{\text{ctr}-1}$  already contains input  $x_i$ , the input of party  $P_i$ .

### Malicious MPC in the $\mathcal{F}_{\text{attest}}$ —hybrid model

The malicious MPC protocol works as follows: Each party  $P_i$  invokes  $\mathcal{F}_{\text{attest}}^{(\text{vk}_i, \text{sk}_i)}$  with the command  $\text{Commit}$  using function  $\pi^*(\cdot)$  described above and sends the received token  $\mathcal{T}_{\pi^*}^{(i)}$  to other parties  $P_j$ . It receives similar tokens  $\mathcal{T}_{\pi^*}^{(j)}$  from party  $P_j$  and verifies it under  $\text{vk}_j$ . Party  $P_i$  aborts if any of these verifications fail. If all verifications succeed, it proceeds with running  $\pi^*(\cdot)$  inside  $\mathcal{F}_{\text{attest}}^{(\text{vk}_i, \text{sk}_i)}$  as described formally in Figure 8.

**Malicious Security.** Next, we prove that if  $\pi$  is secure against semi-honest adversaries, then the protocol described in Figure 8 is an MPC protocol secure against malicious adversaries with the same corruption threshold. For simplicity, consider the case of single malicious party  $P_i$ . Informally, we argue that our technique constrains  $P_i$  to follow the instructions of the semi-honest protocol  $\pi(\cdot)$  faithfully. Or, deviating from faithful execution would result in some honest party to abort. The first  $\text{Compute}$  invocation of  $\mathcal{F}_{\text{attest}}^{(\text{vk}_i, \text{sk}_i)}$  fixes the input of  $P_i$  used in the protocol. Since every other  $\mathcal{F}_{\text{attest}}^{(\text{vk}_j, \text{sk}_j)}$  reliably knows the verification key  $\text{vk}_i$  used by  $\mathcal{F}_{\text{attest}}^{(\text{vk}_i, \text{sk}_i)}$ , it checks the signatures on the function description (i.e.,  $\mathcal{T}_{\pi^*}^{(i)}$ ) as well as the messages of the protocol. The unforgeability of the signature scheme guarantees that  $P_i$  cannot forge signatures on incorrectly generated protocol messages. Note that we use this property to ensure that both of the following signatures cannot be forged: (a) signatures under  $\text{vk}_i$  on messages generated by

### Protocol $\text{Prot}_{\text{malicious}}(P_1, \dots, P_n)$

Party  $P_i$  with input  $x_i$  interacts with  $\{P_j\}_{j \neq i}$  and  $\mathcal{F}_{\text{attest}}^{(\text{vk}_i, \text{sk}_i)}$  and does the following:

- Invokes  $\mathcal{F}_{\text{attest}}^{(\text{vk}_i, \text{sk}_i)}$  on  $(\text{Commit}, \pi^*)$  to receive  $(\text{state}_0^{(i)}, \mathcal{T}_{\pi^*}^{(i)})$  and sends  $\mathcal{T}_{\pi^*}^{(i)}$  to all parties  $P_j$ ,  $j \neq i$ .
- Receives  $\mathcal{T}_{\pi^*}^{(j)}$  from  $P_j$  and runs  $\text{Verify}_{\text{vk}_j}(H(\pi^*), \mathcal{T}_{\pi^*}^{(j)})$  for all  $j \in [n] \setminus i$ . Aborts if one of these checks fail.
- Invokes  $\mathcal{F}_{\text{attest}}^{(\text{vk}_i, \text{sk}_i)}$  on  $(\text{Compute}, x_i)$  to get  $\text{Transcript}_i^1$  containing input  $x_i$ .
- When  $P_i$  receives a message  $M = (y_{\text{ctr}}^{j,i}, \text{ctr}, \sigma)$  from party  $P_j$ , it invokes  $\mathcal{F}_{\text{attest}}^{(\text{vk}_i, \text{sk}_i)}$  on  $(\text{Compute}, (y_{\text{ctr}}^{j,i}, \text{ctr}, \sigma))$  and receives updated transcript or  $\perp$  (and aborts).
- When  $P_i$  needs to send next message to  $P_j$  it invokes  $\mathcal{F}_{\text{attest}}^{(\text{vk}_i, \text{sk}_i)}$  on  $(\text{Compute}, j)$  and receives  $(y_{\text{ctr}}^{i,j}, \text{ctr}, \sigma)$  along with updated transcript and randomness used. Here,  $\sigma$  is a signature on  $(y_{\text{ctr}}^{i,j}, \text{ctr})$  under  $\text{sk}_i$ . It sends  $(y_{\text{ctr}}^{i,j}, \text{ctr}, \sigma)$  to  $P_j$ .
- When  $P_i$  has no more messages to send in  $\pi(\cdot)$ , it computes the output of the function from  $\text{Transcript}_i$ .

Fig. 8: Malicious secure MPC  $\text{Prot}_{\text{malicious}}(P_1, \dots, P_n)$ .

### Functionality $\mathcal{F}_{\text{mpc}}^f(P_1, \dots, P_n)$

$\mathcal{F}_{\text{mpc}}^f$  interacts with parties  $\{P_1, \dots, P_n\}$  and the adversary  $\mathcal{S}$ .

- On input message  $x_i$  from  $P_i$  record  $x_i$  and ignore further  $x_i$  from  $P_i$
- Upon receiving  $x_i$  from all  $P_i$ ,  $i \in [n]$ , compute  $y = f(x_1, \dots, x_n)$  and send to  $\mathcal{S}$ .
- Upon receiving  $(i, \text{Send})$  or  $(i, \perp)$  from  $\mathcal{S}$ , send  $y$  or  $\perp$  to  $P_i$ .

Fig. 9: The MPC functionality  $\mathcal{F}_{\text{mpc}}^f$ .

$\mathcal{F}_{\text{attest}}^{(\text{vk}_i, \text{sk}_i)}$  and sent to honest  $P_j$  (b) signatures under  $\text{vk}_j$  on messages sent by  $P_j$  being fed into  $\mathcal{F}_{\text{attest}}^{(\text{vk}_i, \text{sk}_i)}$ . Also,  $\mathcal{F}_{\text{attest}}^{(\text{vk}_i, \text{sk}_i)}$  provides correct randomness to generate messages of  $P_i$  in the semi-honest secure protocol. Hence, all messages from  $P_i$  to any honest party  $P_j$  are generated correctly as directed by  $\pi$ . This argument can be easily extended to multiple colluding corrupt parties.

Formally, we give a security proof using the standard simulation paradigm (we refer the reader to [26], [16] for details on the paradigm). That is, the protocol in Figure 8 securely realizes the ideal MPC functionality described in Figure 9 against malicious adversaries.

**Theorem 1:** Let  $\pi(\cdot)$  be a semi-honest secure MPC protocol securely realizing  $\mathcal{F}_{\text{mpc}}^f$ . Then, protocol  $\text{Prot}_{\text{malicious}}(P_1, \dots, P_n)$  described in Figure 8 securely realizes  $\mathcal{F}_{\text{mpc}}^f$  in the  $\mathcal{F}_{\text{attest}}^{(\text{vk}_i, \text{sk}_i)}$ —hybrid model (with  $i \in [n]$ ) against malicious adversaries.

*Proof Sketch:* Let  $\mathcal{A}$  be the real world adversary. Ideal world adversary  $\mathcal{S}$  that simulates the view of  $\mathcal{A}$  is as follows: Let  $\mathcal{S}'$  be the ideal world adversary or the semi-honest simulator for  $\pi$  (this exists because  $\pi$  is semi-honest secure).  $\mathcal{S}$  picks  $\{(\text{vk}_k, \text{sk}_k)\}_{k \in [n]}$  and gives  $\{\text{vk}_k\}_{k \in [n]}$  to  $\mathcal{A}$ . We denote a corrupt party by  $P_i$  and honest party by  $P_j$ . Next, when  $\mathcal{A}$  invokes an instance of  $\mathcal{F}_{\text{attest}}^{(\text{vk}_i, \text{sk}_i)}$  on command Commit for a corrupted party  $P_i$ ,  $\mathcal{S}$  simulates the correct behavior of  $\mathcal{F}_{\text{attest}}^{(\text{vk}_i, \text{sk}_i)}$ . Also,  $\mathcal{S}$  sends correctly generated tokens  $\{\mathcal{T}_{\pi^*}^{(j)}\}$  for all honest parties to  $\mathcal{A}$ . When  $\mathcal{S}$  receives token from  $\mathcal{A}$  corresponding to a corrupted party  $P_i$ , it checks it against  $\pi^*$  and  $\text{vk}_i$ . It aborts if verification fails. When  $\mathcal{A}$  invokes  $\mathcal{F}_{\text{attest}}^{(\text{vk}_i, \text{sk}_i)}$  with  $x_i$ ,  $\mathcal{S}$  stores it as input of  $P_i$ . When  $\mathcal{A}$  commits to inputs of all corrupt parties,  $\mathcal{S}$  sends these to  $\mathcal{F}_{\text{mpc}}^f$  to learn output  $y$ . It sends inputs of corrupt parties and output  $y$  to  $\mathcal{S}'$  that generates the view of the adversary in the semi-honest protocol, that contains the randomness for all corrupt parties as well as the transcript of the protocol. Using this, it is easy for  $\mathcal{S}$  to simulate the view of  $\mathcal{A}$  in the rest of the protocol. The indistinguishability of the adversary's view in real and ideal executions follows from the semi-honest security of  $\pi$ . ■

### C. Realizing $\mathcal{F}_{\text{attest}}$ using Intel SGX

SGX allows a host to create a protected region known as an enclave. Intel gives integrity guarantees, that is, the code and the data residing in the enclave, once attested, cannot be modified by the host or the operating system. When SGX receives a Commit command (Figure 7) for a function  $g$ , then it creates an enclave with code  $g$ . Randomness  $r_{\text{ctr}}$  of Figure 7 can be sampled in SGX using `sgx_read_rand` command. The attestation token  $\mathcal{T}_g$  is generated by SGX communicating with Intel's Attestation Service (IAS) and this token is publicly verifiable given  $g$  and public verification key corresponding to Intel's Report Signing Key. The key-pair  $(\text{vk}, \text{sk})$  for ECDSA signature scheme is also generated inside the enclave and the verification key  $\text{vk}$  is sent as payload to IAS during the generation of the attestation token. The token  $\mathcal{T}_g$  contains the verification key  $\text{vk}$  in the clear and this  $\text{vk}$  can be used to verify the signed outputs  $y_{\text{ctr}}$ . Now, on receiving the Compute command, the enclave starts executing the code of  $g$  and produces outputs signed under  $\text{sk}$ .

While running MPC in the  $\mathcal{F}_{\text{attest}}$ -hybrid, we require the enclave to reliably have verification keys used by enclaves of all other parties. This can be done by attaching the following prelude to  $\pi^*$  (the code running inside SGX): Read the tokens of all parties, parse them to obtain the verification keys, and verify the signature on the tokens using verification key of Intel's Report Signing key. Note that since all the parties are running the same function  $\pi^*$  (appended with this prelude), they can compute the hash of  $\pi^*$  locally and compare it with the hash in the tokens (which has been signed by Intel's IAS) of all the other parties, proceeding only if they all match perfectly.

### D. Implementation challenges with SGX

We outline some of the key challenges in implementing MPC between multiple SGX enclaves that involve multiple rounds of interaction and operate over large volumes of data.

*1) Memory constraints in SGX:* In SGX, all the enclave content, including code, and related data is stored in a special region of memory known as the Enclave Page Cache (EPC). The size of EPC is fixed in BIOS and can have a maximum size of 128MB. Typically, paging facilitates the execution of enclaves which cannot fit in EPC and any page that is evicted out is encrypted before storing it on unprotected memory [36]. This additional overhead has detrimental effects on the overall performance of the enclave application. We reduce the working set of secure inference tasks to limit these overheads.

- *ReLU and MaxPool functions:* We split the computation of memory intensive non-linear functions into chunks that fit in EPC to avoid paging. For example, a secure ReLU computation that requires 120MB memory is split into 3 chunks of 40MB each. Note that chunking increases the number of MPC rounds and very small chunks are actually detrimental to performance.
- *Convolution and Matrix Multiplication functions:* For the linear functions, we block the matrices into smaller ones, process the blocks, and aggregate them. We ensure that individual blocks fit in EPC.
- *Liveness Analysis:* Athos implements liveness analysis (Section III-D) which reduces the memory footprint of the compiled DNNs.

*2) Porting Interactive Protocols to SGX:* To the best of our knowledge, we are the first work to implement highly interactive protocols in SGX and this comes with unique challenges. For example, whenever any data is passed across the enclave's protected memory region, it has to be *marshalled* in/out of the region<sup>3</sup>. The performance of marshalling mainly depends on the size of the parameters crossing the bridge. Larger parameters imply slower marshalling [36], while smaller parameters increase the total numbers of cross-bridge calls (which have an overhead of their own). Thus, we tune the payload size carefully. We also implement the techniques in [59] for optimizing communication involving enclaves.

## VI. EXPERIMENTS

**Overview.** In this section, we present our experimental results. First, in Section VI-A, we use CRYPTFLOW to securely compute inference on the ImageNet dataset using the following TensorFlow programs – RESNET50<sup>4</sup>, DENSENET121<sup>5</sup>, and SQUEEZENET<sup>6</sup>. We stress that no prior work has run MPC on networks of this scale. We also show that the performance of semi-honest and malicious protocols generated by CRYPTFLOW scale linearly with the depth of DNNs. Second, in Section VI-B, we show that CRYPTFLOW outperforms prior works on secure inference of DNNs. These experiments are on smaller DNNs that perform prediction over the MNIST and CIFAR10 datasets as prior work could only handle such small benchmarks. Next, we evaluate each

<sup>3</sup>When pointers to memory are passed as parameters into the enclave via an `ecall`, the referenced data block is *marshalled* into the enclave, specifically into the protected memory region that an enclave uses. Similarly, when a pointer to enclave data, residing in protected memory region, is passed outside an enclave via an `ocall`, the referenced data block is marshalled out of the protected memory region.

<sup>4</sup><https://github.com/tensorflow/models/tree/master/official/r1/resnet>

<sup>5</sup><https://github.com/pudae/tensorflow-densenet>

<sup>6</sup><https://github.com/avoroshilov/tf-squeezenet>

component of CRYPTFLOW in more detail. In Section VI-C, we show that the fixed-point code generated by Athos matches the accuracy of floating-point RESNET50, DENSENET121, and SQUEEZENET. We show in Section VI-D how the optimizations in Porthos help it outperform prior works in terms of communication complexity and overall execution time. In Section VI-E, we show the overhead of obtaining malicious secure MPC (over semi-honest security) using Aramis for GMW [26] and Porthos. We show Aramis-based malicious secure inference outperforms pure crypto-based malicious secure protocols by huge margins in Section VI-E1. Finally, in section VI-F, we discuss two case-studies of running CRYPTFLOW on DNNs for healthcare. We begin by providing details of the systems used to run our experiments.

**System Details.** All our large benchmark experiments are in a LAN setting on 3.7GHz machines, each with 4 cores and with 16 GB of RAM running Linux Ubuntu 16.04. The measured bandwidth between each of the machines was at most 377 MBps and the latency was sub millisecond. Since we wanted to use the same machines to benchmark both our semi-honest as well as our malicious secure protocols, we were constrained to use machines that had Intel SGX enabled on them - this led to machines that had considerably lower bandwidth between them (377 MBps) than those normally used by prior works in the area (e.g. [44], [10] used networks with bandwidth of 1.5 GBps). For Aramis, we used Intel SGX SDK version 2.4. We observed that the compilation time of CRYPTFLOW remains under 40 seconds for our benchmarks.

#### A. Secure Inference on ImageNet

In this section, we show the power of CRYPTFLOW, by demonstrating secure inference of RESNET50, DENSENET121, and SQUEEZENET over the ImageNet dataset with over 1000 classes. We briefly describe these DNNs and then present performance results.

- 1) RESNET50 [30] is a network that follows the residual neural network architecture. The residual nodes employs “skip connections” or short cuts between layers. It consists of 53 convolution layers with filters of size upto  $7 \times 7$ , and 1 fully connected layer of size  $2048 \times 1001$ . The activation function between most layers is batch normalization followed by ReLU. After the first convolutional layer, the activation function also includes a MaxPool.
- 2) DENSENET121 [33] is a form of residual neural network that employs several parallel skips. It consists of 121 convolution layers with filters of size upto  $7 \times 7$ . The activation function between these layers is usually batch normalization followed by ReLU. Some layers also use MaxPool or AvgPool.
- 3) SQUEEZENET [35] is a notoriously hard to train network and no prior work has considered evaluating this architecture on ImageNet with fixed-point arithmetic. It consists of 26 convolutional layers with filters of size upto  $3 \times 3$ . The activation function between these layers is usually ReLU and MaxPool.

**Performance.** As shown in Table IV, CRYPTFLOW securely computes the inference over all these state-of-the-art networks within a range of 11–36 seconds with semi-honest security and 29–112 seconds with malicious security. We measure

Benchmark	Semi-Honest (s)	Malicious (s)	Communication (GB)
RESNET50	25.9	75.4	6.9
DENSENET121	36.0	112.9	10.5
SQUEEZENET	11.3	29.0	2.6

TABLE IV: CRYPTFLOW: ImageNet scale benchmarks.

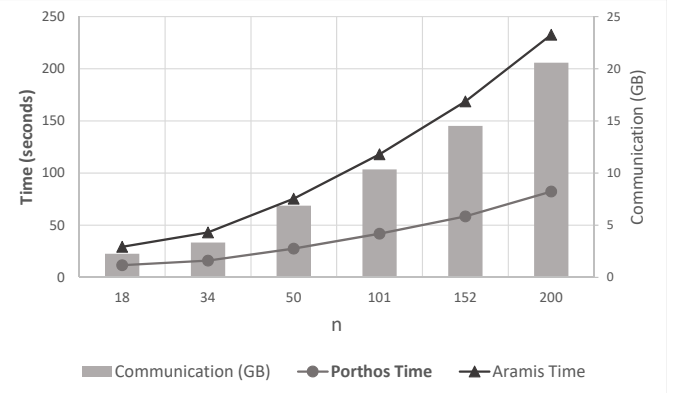


Fig. 10: Scalability of CRYPTFLOW on RESNET-n.

communication as total communication between all 3 parties - each party roughly communicates a third of this value. The communication in semi-honest secure and malicious secure inference is almost the same. Thus demonstrating that ImageNet scale inference can be performed in about 30 seconds with semi-honest security and in under two minutes with malicious security. The malicious security provided by CRYPTFLOW is about 3X more expensive than semi-honest security.

**Scalability.** We show that the running time of CRYPTFLOW-based protocols increases linearly with the depth of DNNs. We compile RESNET- $n$  (where  $n$ , the approximate number of convolutional layers, varies from 18 to 200) with CRYPTFLOW and evaluate with both semi-honest (Porthos) and malicious secure protocols (Aramis) in Figure 10. Our largest benchmark here is RESNET-200, the deepest version of RESNET on the ImageNet dataset [31], which has 65 million parameters. Other RESNET- $n$  benchmarks have between 11 to 60 million parameters<sup>7</sup>. We observe that the communication and runtime increase linearly with depth. Even with increasing depth, the overhead of malicious security (over semi-honest security) remains constant at about 3X.

#### B. Comparison with prior work

In this section, we show that CRYPTFLOW outperforms prior works on secure inference of DNNs on the benchmarks they consider, i.e., tiny 2–4 layer DNNs over the MNIST and CIFAR-10 datasets. We stress that these benchmarks are very small compared to the ImageNet scale DNNs discussed above. In order to provide a fair comparison, for these experiments, we use a network with similar bandwidth as prior works (1.5 GBps) and machines with similar compute (2.7 GHz).

Table V compares Porthos with prior (ABY<sup>3</sup> [44] and SecureNN [61]) and concurrent (QuantizedNN [10]) semi-honest secure 3PC works on the MNIST dataset. Table VI

<sup>7</sup>Specifically, 11, 22, 25, 44 and 60 million parameters for RESNET- $n$  for  $n = 18, 34, 50, 101$ , and 152 respectively.

Benchmark	ABY3	Quantized NN	SecureNN	Porthos
Logistic Regression	4	—	—	2.7
SecureML (3 layer DNN)	8	20	17	8
MiniONN (4 layer CNN)	-	80	47	34
LeNet (4 layer CNN)	-	120	79	58

TABLE V: Comparison with 3PC on MNIST dataset – All times in milliseconds.

Benchmark	CHET	MiniONN	EzPC	Gazelle	Porthos
SQUEEZE NET* (CIFAR)	1342	-	-	-	0.05
MiniONN (CIFAR)	-	544	265.6	12.9	0.36
MiniONN (MNIST)	-	9.4	5.1	0.81	0.03

TABLE VI: Comparison with 2PC – All times in seconds. CHET replaces ReLUs in a small SQUEEZE NET with square activations.

compares Porthos with prior 2PC work. We omit some prior works (e.g., [45], [15], [55], etc.) in these tables as they are slower than Gazelle and do not provide additional insights. As can be seen from the tables, the 2PC systems are much slower than the 3PC systems and Porthos performs better than other 3PC systems. For instance, for a 4-layer CNN for MNIST from MiniONN [42], the best 2PC-backend Gazelle takes 810 ms, prior best 3PC work takes 47 ms, and Porthos takes 34 ms.

#### C. Athos experiments

**Accuracy of Float-to-Fixed.** We show that Athos generated fixed-point code matches the accuracy of floating-code on RESNET50, DENSENET121, and SQUEEZE NET in Table VII. The table also shows the precision or the scale that is selected by Athos (Section III-B). We observe that different benchmarks require different precision to maximize the classification accuracy and that the technique of “sweeping” through various precision levels is effective. We show how accuracy varies with precision in Appendix B. Evaluating accuracy also helps validate the correctness of our compilation [46].

**Modularity.** Since CRYPTFLOW is modular, we can compile it to various MPC backends. To demonstrate this ability, we also add a 2PC semi-honest secure protocol ABY [22] to CRYPTFLOW. The performance with this backend is in Table VIII. We ran logistic regression (LR) as well as a small LeNet network [40] which comprises of 2 convolutional layers (with maximum filter size of  $5 \times 5$ ) and 2 fully connected layers, with ReLU and MaxPool as the activation functions. This evaluation shows that CRYPTFLOW can be easily used for a variety of backends - however the current state-of-the-art performance of 2PC makes it difficult to execute the large DNNs described in Section VI-A. One could potentially implement the functions in Table II with state-of-the-art 2PC backends such as Gazelle [38]. The codebase of Gazelle is not publicly available and hence we could not do the same.

Benchmark	Float Top 1	Fixed Top 1	Float Top 5	Fixed Top 5	Scale
RESNET50	76.47	76.45	93.21	93.23	12
DENSENET121	74.25	74.33	91.88	91.90	11
SQUEEZE NET	55.86	55.92	79.18	79.24	10

TABLE VII: Accuracy of fixed-point vs floating-point.

Benchmark	CRYPTFLOW (s)	Communication (MB)
LogisticRegression	0.227	25.5
LeNet Small	47.4	2939

TABLE VIII: CRYPTFLOW compilation to 2PC on MNIST.

Benchmark	SecureNN (s)	Porthos (s)	SecureNN Comm. (GB)	Porthos Comm. (GB)
RESNET50	38.36	25.87	8.54	6.87
DENSENET121	53.99	36.00	13.53	10.54
SQUEEZE NET	16.55	11.28	3.88	2.63

TABLE IX: Porthos vs SecureNN.

#### D. Porthos experiments

Since Porthos improves SecureNN, we compare them in mode detail. As described earlier, Porthos improves over the communication complexity of SecureNN [61] both for convolutional layers as well as for non-linear activation functions. We have already compared SecureNN and Porthos on benchmarks considered in SecureNN in Table V. Additionally, we also compare Porthos and SecureNN on ImageNet scale benchmarks in Table IX. For this purpose, we add the code of SecureNN available at [60] as another backend to CRYPTFLOW. These results show that Porthos improves upon the communication of SecureNN by a factor of roughly 1.2X–1.5X and the runtime by a factor of roughly 1.4X–1.5X.

#### E. Aramis experiments

We ported both the 2-party GMW protocol [26] (using the codebase [34], based on [19]) as well as Porthos into Intel SGX. The results for different functions using the GMW protocol are presented in Table X.  $\text{IP}_n$  denotes the inner product of two  $n$ -element vectors over  $\mathbb{F}_2$ ,  $\text{Add}_{32}$  and  $\text{Mult}_{32}$  denote addition and multiplication over 32 bits respectively, and  $\text{Millionaire}_{32}$  denotes the millionaires problem that compares two 32-bit integers  $x$  and  $y$  and outputs a single bit denoting whether  $x > y$ . Aramis in this table denotes the semi-honest GMW protocol ported into Intel SGX to provide malicious security.

As can be seen, all overheads in this case, are within 54% of the semi-honest protocol. Since these benchmarks are small, all of the code and data fit inside the SGX enclave without any requirement for paging and hence overheads are also minimal. For ImageNet scale benchmarks, the overheads are higher (Table IV). Since these benchmarks are much larger, we have to deal with well-known paging issues that occur when using Intel SGX with large data [36]; here we incur overheads of about 3X over semi-honest protocols.

*1) Comparison with crypto-only malicious MPC:* We demonstrate that Aramis based malicious secure protocols are better suited for large scale inference tasks compared to pure cryptographic solutions. We compare the performance of Porthos compiled with Aramis and the concurrent work of QuantizedNN [10] that uses the MP-SPDZ [39] framework to also provide a malicious secure variant of their protocol. Both these approaches provide security for the same setting of 3PC with 1 corruption. On the four MNIST inference benchmarks A/B/C/D in the MP-SPDZ repository, Aramis is 10X/46X/44X/15X faster. Furthermore, in these performance measurements, we are being unfair to Aramis: MP-SPDZ strips out all the ReLUs from its performance estimates and its performance would be much worse in their presence. However,

Benchmark	GMW (ms)	Aramis (ms)	Overhead
$\text{IP}_{10,000}$	464	638	1.37x
$\text{IP}_{100,000}$	2145	3318	1.54x
$\text{Add}_{32}$	279	351	1.25x
$\text{Mult}_{32}$	354	461	1.30x
$\text{Millionaire}_{32}$	292	374	1.28x

TABLE X: Semi-honest GMW vs Malicious Aramis.

the Aramis time measurements include the time to compute ReLUs, which can be 80% of the total execution time. If one were to evaluate ReLUs with MP-SPDZ then the speedups of Aramis would be even higher.

#### F. Real world impact

We discuss our experience with using CRYPTFLOW to compile and run DNNs used in healthcare. These DNNs are available as pretrained Keras models. We converted them into TensorFlow using [4] and compiled the automatically generated TensorFlow code with CRYPTFLOW.

*a) Chest X-Ray:* In [63], the authors train a DENSENET121 to predict lung diseases from chest X-ray images. They use the publicly available NIH dataset of chest X-ray images and end up achieving an average AUROC score of 0.845 across 14 possible disease labels. During secure inference, we observed no loss in accuracy and the runtime is similar to the runtime of DENSENET121 for ImageNet.

*b) Diabetic Retinopathy CNN:* Diabetic Retinopathy (DR), one of the major causes of blindness, is a medical condition which leads to damage of retina due to diabetes [47]. In recent times, major tech companies have taken an interest in using DNNs for diagnosing DR from retinal images [47], [28]. Predicting whether a retina image has DR or not can be done securely in about 30 seconds with CRYPTFLOW.

## VII. RELATED WORK

**High level languages.** CRYPTFLOW is the first system to compile high level TensorFlow code to secure MPC protocols. There have been prior works that compile from lower-level, domain-specific languages to MPC. Examples include Fairplay [43], Wysteria [53], ObliVM [41], CBMC-GC [32], SMCL [49], Sharemind [13], EzPC [17], SPDZ [7], and HyCC [15]. Reimplementing DNNs in the input format of these tools is a formidable task. In particular, the float-to-fixed compilation must be done manually by a user of these frameworks. Thus, prior systems fall short of providing the type of support required to run realistic ML benchmarks.

**Fixed-point in MPC.** Although the use of fixed-point for secure computations is well-known [51], prior works on secure inference have addressed the float-to-fixed problem by either generating a fixed-point model by hand ([45], [42], [38], [44], [61]), or by using non-standard training algorithms that output fixed-point models ([54], [5]). Both of these approaches are unsatisfactory. In particular, some of the challenges that one would face with the latter include: a) the need to train again on the whole training data which is both computationally expensive, and impossible if the training data is unavailable; and b) training algorithms that generate integer models is still an active research area and an overwhelming majority of ML training algorithms still generate floating-point

models. Athos alleviates all these problems by working with a trained model and being completely oblivious to the training procedure. The ML users can train their networks in the manner they see fit and then use Athos to get fixed-point code.

**Float-to-fixed.** The research literature in float-to-fixed for digital signal processors is rich and spans several decades. However, it is only recently that these schemes have been adapted to machine learning. Some recent float-to-fixed schemes [27], [48] show promise by quantizing floating-point models to 8-bit or 16-bit integers. One could potentially use one of these systems in place of our float-to-fixed component – however, their compatibility with MPC protocols is unclear. Additionally, since we use higher bit-width of 64, not surprisingly, the accuracy of CRYPTFLOW is better. Another approach is to use TensorFlow’s “post-training-quantization” support that converts a floating-point model to a model over 8-bit and 32-bit integers. However, at inference time, to preserve accuracy, all operations are still performed in floating-point arithmetic, which are very slow in MPC (Table I). Similarly, the quantized SQUEEZENET [35] models are stored as integers but are converted to floating-point at inference time.

**Secure Machine Learning.** There has been a flurry of recent results in the area of secure machine learning, both in the 2-party [14], [50], [25], [42], [38], as well as in the 3-party setting [55], [44], [61], [10]. The most relevant to our work are ABY<sup>3</sup> [44] and SecureNN [61] that both provide 3-party semi-honest secure computation protocols for a variety of neural network inference and training algorithms, with somewhat similar performance guarantees. As we show later, Porthos, our 3-party semi-honest protocol, outperforms both these works. We also remark that there have been other recent works [54], [57], [5], [24], [20], [12], that modify the inference or training algorithms in order to obtain performance benefits. These are applicable only to specialized benchmarks. For example, the works that use fully homomorphic encryption (e.g., [20], [12]) do not support ReLUs. On the other hand, we focus on standard inference algorithms and CRYPTFLOW has much wider applicability.

**Hardware-based security.** Our work is the first to provide experimentally validated malicious secure inference of ML algorithms at the scale of RESNET50. As discussed earlier, we achieve this by relying on minimally secure hardware to provide code attestation and integrity. Prior works that use hardware enclaves for secure computation [56], [52], [29], [9], [18] assume that the enclave hides all data residing in it from the host. The only prior work that assumes a weaker trust assumption from the hardware is that of Tramèr *et al.* [59]. Similar to our work, they assume that the hardware provides code attestation and integrity. However, their work is in the context of zero-knowledge proofs and other fundamentally asymmetric primitives that require only one enclave and not interactive protocols between multiple enclaves.

## VIII. CONCLUSION

CRYPTFLOW is the first end-to-end system from a high level framework, TensorFlow, to MPC protocols. It comes with 3 important components - a) Athos, the float-to-fixed compiler which matches the accuracy of floating-point DNNs, b) an

improved semi-honest 3-party secure computation protocol for DNNs, and c) a generic technique to convert semi-honest secure protocols to maliciously secure ones that makes a minimal trust assumption in hardware. We demonstrate the first instance of secure inference on large benchmarks such as RESNET50 and DENSENET121 on the ImageNet dataset with both semi-honest (in about thirty seconds) and malicious security (in less than two minutes). CRYPTFLOW easily supports a variety of backend crypto protocols and we believe that it can serve as the benchmark framework for future works in the area. In the future, we would like to consider compiling TensorFlow training code as well. However, none of the existing MPC protocols [45], [61], [44] for training have GPU support and thus the overheads of secure training are huge.

## REFERENCES

[1] “Tensorflow graph transform tool,” [https://github.com/tensorflow/tensorflow/blob/master/tensorflow/tools/graph\\_transforms/README.md](https://github.com/tensorflow/tensorflow/blob/master/tensorflow/tools/graph_transforms/README.md).

[2] “Tensorflow tutorial: Convolutional neural networks,” [https://www.tensorflow.org/beta/tutorials/images/intro\\_to\\_cnns](https://www.tensorflow.org/beta/tutorials/images/intro_to_cnns).

[3] M. Abadi, A. Agarwal, P. Barham, E. Brevdo, Z. Chen, C. Citro, G. S. Corrado, A. Davis, J. Dean, M. Devin, S. Ghemawat, I. J. Goodfellow, A. Harp, G. Irving, M. Isard, Y. Jia, R. Józefowicz, L. Kaiser, M. Kudlur, J. Levenberg, D. Mané, R. Monga, S. Moore, D. G. Murray, C. Olah, M. Schuster, J. Shlens, B. Steiner, I. Sutskever, K. Talwar, P. A. Tucker, V. Vanhoucke, V. Vasudevan, F. B. Viégas, O. Vinyals, P. Warden, M. Wattenberg, M. Wicke, Y. Yu, and X. Zheng, “Tensorflow: Large-scale machine learning on heterogeneous distributed systems,” *CoRR*, vol. abs/1603.04467, 2016.

[4] A. Abdi, “Keras to tensorflow,” [https://github.com/amir-abdi/keras\\_to\\_tensorflow](https://github.com/amir-abdi/keras_to_tensorflow), 2019.

[5] N. Agarwal, A. Gascon, A. S. Shamsabadi, and M. Kusne, “Quotient : Two-party secure neural network training and prediciton,” 2019.

[6] A. V. Aho, M. S. Lam, R. Sethi, and J. D. Ullman, *Compilers: Principles, Techniques, and Tools (2Nd Edition)*. Boston, MA, USA: Addison-Wesley Longman Publishing Co., Inc., 2006.

[7] T. Araki, A. Barak, J. Furukawa, M. Keller, Y. Lindell, K. Ohara, and H. Tsuchida, “Generalizing the SPDZ compiler for other protocols,” in *Proceedings of the 2018 ACM SIGSAC Conference on Computer and Communications Security, CCS 2018, Toronto, ON, Canada, October 15-19, 2018*, 2018, pp. 880–895.

[8] T. Araki, J. Furukawa, Y. Lindell, A. Nof, and K. Ohara, “High-throughput semi-honest secure three-party computation with an honest majority,” in *Proceedings of the 2016 ACM SIGSAC Conference on Computer and Communications Security, Vienna, Austria, October 24-28, 2016*, 2016, pp. 805–817. [Online]. Available: <https://doi.org/10.1145/2976749.2978331>

[9] R. Bahmani, M. Barbosa, F. Brassier, B. Portela, A. Sadeghi, G. Scerri, and B. Warinschi, “Secure multiparty computation from SGX,” in *Financial Cryptography and Data Security - 21st International Conference, FC 2017, Sliema, Malta, April 3-7, 2017, Revised Selected Papers*, 2017, pp. 477–497.

[10] A. Barak, D. Escudero, A. Dalskov, and M. Keller, “Secure evaluation of quantized neural networks,” *Cryptology ePrint Archive*, Report 2019/131, 2019, <https://eprint.iacr.org/2019/131>.

[11] D. Beaver, “Efficient multiparty protocols using circuit randomization,” in *Advances in Cryptology - CRYPTO '91, 11th Annual International Cryptology Conference, Santa Barbara, California, USA, August 11-15, 1991, Proceedings*, 1991, pp. 420–432. [Online]. Available: [https://doi.org/10.1007/3-540-46766-1\\_34](https://doi.org/10.1007/3-540-46766-1_34)

[12] F. Boemer, Y. Lao, R. Cammarota, and C. Wierzyński, “nGraph-HE: A graph compiler for deep learning on homomorphically encrypted data,” in *Proceedings of the 16th ACM International Conference on Computing Frontiers*, ser. CF '19.

[13] D. Bogdanov, S. Laur, and J. Willemson, “Sharemind: A framework for fast privacy-preserving computations,” in *Computer Security - ESORICS 2008, 13th European Symposium on Research in Computer Security, Málaga, Spain, October 6-8, 2008. Proceedings*, 2008, pp. 192–206. [Online]. Available: [https://doi.org/10.1007/978-3-540-88313-5\\_13](https://doi.org/10.1007/978-3-540-88313-5_13)

[14] R. Bost, R. A. Popa, S. Tu, and S. Goldwasser, “Machine learning classification over encrypted data,” in *NDSS*, 2015.

[15] N. Büscher, D. Demmler, S. Katzenbeisser, D. Kretzmer, and T. Schneider, “Hycc: Compilation of hybrid protocols for practical secure computation,” in *Proceedings of the 2018 ACM SIGSAC Conference on Computer and Communications Security, CCS 2018, Toronto, ON, Canada, October 15-19, 2018*, 2018, pp. 847–861.

[16] R. Canetti, “Security and composition of multiparty cryptographic protocols,” *J. Cryptology*, vol. 13, no. 1, pp. 143–202, 2000. [Online]. Available: <https://doi.org/10.1007/s001459910006>

[17] N. Chandran, D. Gupta, A. Rastogi, R. Sharma, and S. Tripathi, “EzPC: Programmable and efficient secure two-party computation for machine learning,” in *2019 IEEE European Symposium on Security and Privacy, EuroS&P 2019*, 2019.

[18] J. I. Choi, D. J. Tian, G. Hernandez, C. Patton, B. Mood, T. Shrimpton, K. R. B. Butler, and P. Traynor, “A hybrid approach to secure function evaluation using sgx,” in *Proceedings of the 2019 ACM Asia Conference on Computer and Communications Security*, ser. Asia CCS '19.

[19] S. G. Choi, K. Hwang, J. Katz, T. Malkin, and D. Rubenstein, “Secure multi-party computation of boolean circuits with applications to privacy in on-line marketplaces,” in *Topics in Cryptology - CT-RSA 2012 - The Cryptographers' Track at the RSA Conference 2012, San Francisco, CA, USA, February 27 - March 2, 2012. Proceedings*, 2012, pp. 416–432.

[20] R. Dathathri, O. Saarikivi, H. Chen, K. Lauter, S. Maleki, M. Musuvathi, and T. Mytkowicz, “CHET: An optimizing compiler for fully-homomorphic neural-network inferencing,” in *Proceedings of the 40th ACM SIGPLAN Conference on Programming Language Design and Implementation, PLDI 2019, Phoenix, AZ, USA, June 22-26, 2019*, 2019.

[21] D. Demmler, G. Dessaouky, F. Koushanfar, A. Sadeghi, T. Schneider, and S. Zeitouni, “Automated synthesis of optimized circuits for secure computation,” in *ACM CCS*, 2015.

[22] D. Demmler, T. Schneider, and M. Zohner, “ABY - A framework for efficient mixed-protocol secure two-party computation,” in *NDSS*, 2015.

[23] J. Deng, W. Dong, R. Socher, L. Li, K. Li, and F. Li, “Imagenet: A large-scale hierarchical image database,” in *2009 IEEE Computer Society Conference on Computer Vision and Pattern Recognition (CVPR 2009), 20-25 June 2009, Miami, Florida, USA*, 2009, pp. 248–255.

[24] S. Garg, Z. Ghodsi, C. Hazay, Y. Ishai, A. Marcedone, and M. Venkitasubramaniam, “Outsourcing private machine learning via lightweight secure arithmetic computation,” *CoRR*, vol. abs/1812.01372, 2018. [Online]. Available: <http://arxiv.org/abs/1812.01372>

[25] R. Gilad-Bachrach, N. Dowlin, K. Laine, K. E. Lauter, M. Naehrig, and J. Wernsing, “Cryptonets: Applying neural networks to encrypted data with high throughput and accuracy,” in *ICML*, 2016.

[26] O. Goldreich, S. Micali, and A. Wigderson, “How to play any mental game or A completeness theorem for protocols with honest majority,” in *STOC*, 1987.

[27] S. Gopinath, N. Ghanathe, V. Seshadri, and R. Sharma, “Compiling kb-sized machine learning models to tiny iot devices,” in *Proceedings of the 40th ACM SIGPLAN Conference on Programming Language Design and Implementation, PLDI 2019, Phoenix, AZ, USA, June 22-26, 2019*, 2019.

[28] V. Gulshan, L. Peng, M. Coram, M. C. Stumpe, D. Wu, A. Narayanaswamy, S. Venugopalan, K. Widner, T. Madams, J. Cuadros, R. Kim, R. Raman, P. C. Nelson, J. L. Mega, and D. R. Webster, “Development and Validation of a Deep Learning Algorithm for Detection of Diabetic Retinopathy in Retinal Fundus PhotographsAccuracy of a Deep Learning Algorithm for Detection of Diabetic RetinopathyAccuracy of a Deep Learning Algorithm for Detection of Diabetic Retinopathy,” *JAMA*, vol. 316, no. 22, pp. 2402–2410, 12 2016. [Online]. Available: <https://doi.org/10.1001/jama.2016.17216>

[29] D. Gupta, B. Mood, J. Feigenbaum, K. R. B. Butler, and P. Traynor, “Using intel software guard extensions for efficient two-party secure function evaluation,” in *Financial Cryptography and Data Security - FC 2016 International Workshops, BITCOIN, VOTING, and WAHC, Christ Church, Barbados, February 26, 2016, Revised Selected Papers*, 2016, pp. 302–318.

[30] K. He, X. Zhang, S. Ren, and J. Sun, "Deep residual learning for image recognition," in *2016 IEEE Conference on Computer Vision and Pattern Recognition, CVPR 2016, Las Vegas, NV, USA, June 27-30, 2016*, 2016, pp. 770–778.

[31] —, "Identity mappings in deep residual networks," in *European conference on computer vision*. Springer, 2016, pp. 630–645.

[32] A. Holzer, M. Franz, S. Katzenbeisser, and H. Veith, "Secure two-party computations in ANSI C," in *the ACM Conference on Computer and Communications Security, CCS'12, Raleigh, NC, USA, October 16-18, 2012*, 2012, pp. 772–783.

[33] G. Huang, Z. Liu, L. van der Maaten, and K. Q. Weinberger, "Densely connected convolutional networks," in *2017 IEEE Conference on Computer Vision and Pattern Recognition, CVPR 2017, Honolulu, HI, USA, July 21-26, 2017*, 2017, pp. 2261–2269.

[34] K.-W. Hwang, "GMW codebase," 2012. [Online]. Available: <http://www.ee.columbia.edu/~khwang/projects/gmw.html>

[35] F. N. Iandola, M. W. Moskewicz, K. Ashraf, S. Han, W. J. Dally, and K. Keutzer, "SqueezeNet: Alexnet-level accuracy with 50x fewer parameters and <1mb model size," *CoRR*, vol. abs/1602.07360, 2016. [Online]. Available: <http://arxiv.org/abs/1602.07360>

[36] Intel, "Performance considerations for intel software guard extensions (intel SGX) applications," 2018. [Online]. Available: <https://software.intel.com/sites/default/files/managed/09/37/Intel-SGX-Performance-Considerations.pdf>

[37] —, "Intel SGX SDK," 2019. [Online]. Available: <https://software.intel.com/en-us/sgx/sdk>

[38] C. Juvekar, V. Vaikuntanathan, and A. Chandrakasani, "GAZELLE: A low latency framework for secure neural network inference," in *USENIX Security 18*, 2018.

[39] M. Keller, "Multi-protocol spdz: Versatile framework for multi-party computation," 2019. [Online]. Available: <https://github.com/data61/MP-SPDZ>

[40] Y. Lecun, L. Bottou, Y. Bengio, and P. Haffner, "Gradient-based learning applied to document recognition," in *Proceedings of the IEEE, 1998*, pp. 2278–2324.

[41] C. Liu, X. S. Wang, K. Nayak, Y. Huang, and E. Shi, "Oblivm: A programming framework for secure computation," in *2015 IEEE Symposium on Security and Privacy, SP 2015, San Jose, CA, USA, May 17-21, 2015*, 2015, pp. 359–376. [Online]. Available: <https://doi.org/10.1109/SP.2015.29>

[42] J. Liu, M. Juuti, Y. Lu, and N. Asokan, "Oblivious neural network predictions via minionn transformations," in *CCS*, 2017.

[43] D. Malkhi, N. Nisan, B. Pinkas, and Y. Sella, "Fairplay - secure two-party computation system," in *Proceedings of the 13th USENIX Security Symposium, August 9-13, 2004, San Diego, CA, USA, 2004*, pp. 287–302. [Online]. Available: <http://www.usenix.org/publications/library/proceedings/sec04/tech/malkhi.html>

[44] P. Mohassel and P. Rindal, "Aby<sup>3</sup>: A mixed protocol framework for machine learning," in *Proceedings of the 2018 ACM SIGSAC Conference on Computer and Communications Security, CCS 2018, Toronto, ON, Canada, October 15-19, 2018*, 2018, pp. 35–52.

[45] P. Mohassel and Y. Zhang, "Secureml: A system for scalable privacy-preserving machine learning," in *IEEE S&P*, 2017.

[46] B. Mood, D. Gupta, H. Carter, K. R. B. Butler, and P. Traynor, "Frigate: A validated, extensible, and efficient compiler and interpreter for secure computation," in *IEEE EuroS&P*, 2016.

[47] J. MSV, "Google's research in artificial intelligence helps in preventing blindness caused by diabetes," *Forbes*, sep 2017.

[48] M. Nagel, M. van Baalen, T. Blankevoort, and M. Welling, "Data-free quantization through weight equalization and bias correction," *CoRR*, vol. abs/1906.04721, 2019. [Online]. Available: <http://arxiv.org/abs/1906.04721>

[49] J. D. Nielsen and M. I. Schwartzbach, "A domain-specific programming language for secure multiparty computation," in *Proceedings of the 2007 Workshop on Programming Languages and Analysis for Security, PLAS 2007, San Diego, California, USA, June 14, 2007*, 2007, pp. 21–30. [Online]. Available: <http://doi.acm.org/10.1145/1255329.1255333>

[50] V. Nikolaenko, S. Ioannidis, U. Weinsberg, M. Joye, N. Taft, and D. Boneh, "Privacy-preserving matrix factorization," in *ACM CCS*, 2013.

[51] V. Nikolaenko, U. Weinsberg, S. Ioannidis, M. Joye, D. Boneh, and N. Taft, "Privacy-preserving ridge regression on hundreds of millions of records," in *IEEE S&P*, 2013.

[52] O. Ohrimenko, F. Schuster, C. Fournet, A. Mehta, S. Nowozin, K. Vaswani, and M. Costa, "Oblivious multi-party machine learning on trusted processors," in *25th USENIX Security Symposium, USENIX Security 16, Austin, TX, USA, August 10-12, 2016*, 2016, pp. 619–636.

[53] A. Rastogi, M. A. Hammer, and M. Hicks, "Wysteria: A programming language for generic, mixed-mode multiparty computations," in *2014 IEEE Symposium on Security and Privacy, SP 2014, Berkeley, CA, USA, May 18-21, 2014*, 2014, pp. 655–670.

[54] M. S. Riazi, M. Samragh, H. Chen, K. Laine, K. Lauter, and F. Koushanfar, "Xonn: Xnor-based oblivious deep neural network inference," in *28th USENIX Security Symposium, USENIX Security 2019*, 2019.

[55] M. S. Riazi, C. Weinert, O. Tkachenko, E. M. Songhori, T. Schneider, and F. Koushanfar, "Chameleon: A hybrid secure computation framework for machine learning applications," in *ASIACCS*, 2018.

[56] F. Schuster, M. Costa, C. Fournet, C. Gkantsidis, M. Peinado, G. Mainar-Ruiz, and M. Russinovich, "VC3: trustworthy data analytics in the cloud using SGX," in *2015 IEEE Symposium on Security and Privacy, SP 2015, San Jose, CA, USA, May 17-21, 2015*, 2015, pp. 38–54.

[57] J. So, B. Guler, A. S. Avestimehr, and P. Mohassel, "Codedprivateml: A fast and privacy-preserving framework for distributed machine learning," *Cryptology ePrint Archive, Report 2019/140*, 2019, <https://eprint.iacr.org/2019/140>.

[58] TensorFlow, "Broadcasting semantics," <https://www.tensorflow.org/xla/broadcasting>, 2018.

[59] F. Tramèr, F. Zhang, H. Lin, J. Hubaux, A. Juels, and E. Shi, "Sealed-glass proofs: Using transparent enclaves to prove and sell knowledge," in *2017 IEEE European Symposium on Security and Privacy, EuroS&P 2017, Paris, France, April 26-28, 2017*, 2017, pp. 19–34.

[60] S. Wagh, "SecureNN codebase," 2019. [Online]. Available: <https://github.com/snwagh/securenn-public>

[61] S. Wagh, D. Gupta, and N. Chandran, "Securenn: 3-party secure computation for neural network training," *PoPETs*, vol. 2019, no. 3, 2019.

[62] A. C. Yao, "How to generate and exchange secrets (extended abstract)," in *FOCS*, 1986.

[63] X. Zhu, G. Iordanescu, I. Karmanov, and M. Zawaideh, Mar 2018. [Online]. Available: <https://blogs.technet.microsoft.com/machinelearning/2018/03/07/using-microsoft-ai-to-build-a-lung-disease-prediction-model-using-chest-x-ray-im>

## APPENDIX

### A. Algorithms used by Porthos

The additional algorithms that reshape filters, input, and output, used by Porthos are described in Algorithms 2, 3, and 4.

#### Algorithm 2: ReshapeFilter

---

**Input:**  $X \in \mathbb{Z}_L^{f \times f}$ .  
**Output:**  $Z \in \mathbb{Z}_L^{f^2 \times 1}$ .  
1. **for**  $i = \{0, \dots, f - 1\}$  **do**  
2.     **for**  $j = \{0, \dots, f - 1\}$  **do**  
3.          $Z[i \cdot f + j] = X[i][j]$   
4.     **end for**  
5. **end for**

---

#### Algorithm 3: ReshapeInput

---

**Input:**  $X \in \mathbb{Z}_L^{m \times m}$ .  
**Output:**  $Z \in \mathbb{Z}_L^{n^2 \times f^2}$  where  $n = m - f + 1$ .  
**Global Information:** Filter dimension  $f$ .  
1. **for**  $i = \{0, \dots, m - f\}$  **do**  
2.     **for**  $j = \{0, \dots, m - f\}$  **do**  
3.         **for**  $k = \{0, \dots, f - 1\}$  **do**  
4.             **for**  $l = \{0, \dots, f - 1\}$  **do**  
5.                  $Z[i \cdot (m - f + 1) + j][k \cdot f + j] = X[k + i][l + j]$   
6.             **end for**  
7.         **end for**  
8.     **end for**  
9. **end for**

---

#### Algorithm 4: ReshapeOutput

---

**Input:**  $X \in \mathbb{Z}_L^{n^2 \times 1}$ .  
**Output:**  $Z \in \mathbb{Z}_L^{n \times n}$ .  
1. **for**  $i = \{0, \dots, n - 1\}$  **do**  
2.     **for**  $j = \{0, \dots, n - 1\}$  **do**  
3.          $Z[i][j] = X[i \cdot n + j]$   
4.     **end for**  
5. **end for**

---

### B. Accuracy of Athos

In this section, we present the Top 1 and Top 5 accuracies of Athos on ImageNet dataset.

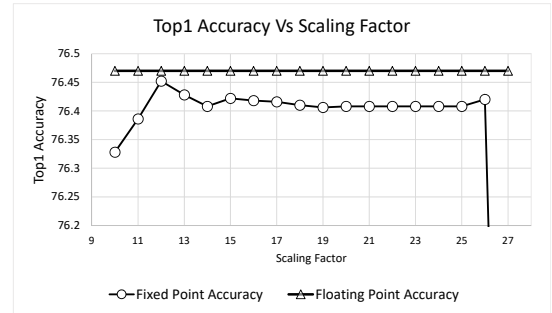


Fig. 11: RESNET50: Top 1 accuracy vs Scale

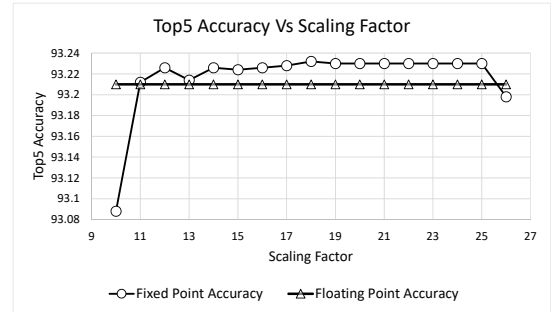


Fig. 12: RESNET50: Top 5 accuracy vs Scale

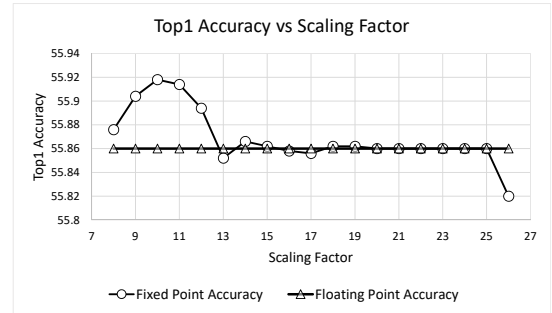


Fig. 13: SQUEEZENET: Top 1 accuracy vs Scale

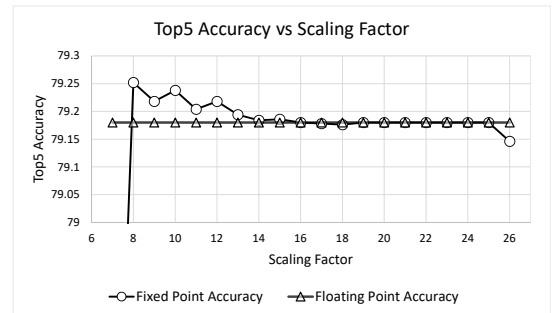


Fig. 14: SQUEEZENET: Top 5 accuracy vs Scale

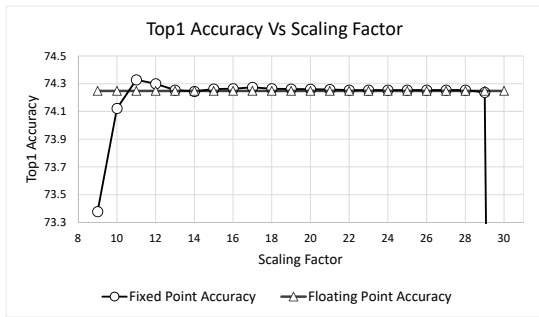


Fig. 15: DENSENET121: Top 1 accuracy vs Scale

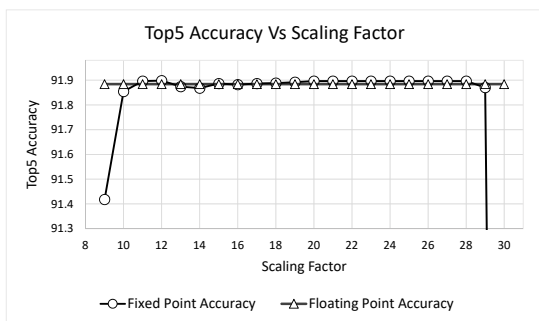


Fig. 16: DENSENET121: Top 5 accuracy vs Scale